THE WHOLE-CORE LEU U_3Si_2-AL FUEL DEMONSTRATION IN THE 30-MW OAK RIDGE RESEARCH REACTOR

1. INTRODUCTION

Early in the history of the U.S. Reduced Enrichment Research and Test Reactor (RERTR) Program the need for a whole-core demonstration of high uranium density LEU fuel was recognized. Plate-type U_3Si_2-Al dispersion fuel was chosen for the demonstration because of its excellent behavior under irradiation[1], its high maximum practical uranium density (4.8 gU/cc), and its ease of fabrication by commercial suppliers. The primary objectives of the demonstration were:

1. to demonstrate the safe and acceptable behavior of commercially-fabricated 20%-enriched U_3Si_2-Al dispersion fuel (4.8 g U/cc in fuel meat) to average ^{235}U burnups greater than 50% in a relatively high power research reactor.

2. to demonstrate the safe transition process from an all-HEU equilibrium core, through a series of mixed HEU/LEU cores, to an all-LEU equilibrium. core, and

3. to provide an abundance of core physics data for validating analytical methods, codes and burnup predictions.

The 30-MW Oak Ridge Research Reactor (ORR) was chosen for the demonstration because its high power would provide data for the validation of fuel cycle calculations in relatively short times and because analyses showed that the demonstration would cause only minor changes in the performance of standard ORR experiments. Three international fuel vendors fabricated the U_3Si_2-AI LEU elements for the ORR demonstration. Sixty fuel elements and twelve shim rod assemblies were fabricated by Babcock and Wilcox (USA), and twenty elements each were supplied by CERCA (France) and NUKEM (FRG). Each 19-plate 20%-enriched fuel element had a meat density of 4.8 g U/cc and contained 340 g ^{235}U. The 15-plate fuel followers had a density of 3.5 g U/cc and contained 200 9 ^{235}U. HEU (U_30_8-Al) and LEU fuel elements are of identical geometry.

The demonstration began with an all-HEU reference core (174C) in December 1985. The first three LEU elements were phased into the ORR core (174D) at the beginning of January 1986. Following every cycle thereafter three or four fresh LEU elements were inserted on the outer edge of the core, an equal number of spent HEU elements were discharged from the center of the core, and the remaining elements were redistributed throughout the core. Normally, the ORR operated with two nearly identical cores which were alternated between the reactor and the pool to allow for xenon decay. The first all-LEU core (178C) operated in December 1986. With the completion of cycle 179A, the ORR was permanently shut down in March 1987 for reasons entirely unrelated to the demonstration. In all, 22 cores were operated at full power during the course of the demonstration.

Because of the unexpected shutdown, not as many LEU fuel elements were fully irradiated as had been planned initially. Nevertheless, the primary objectives of the demonstration, as stated above, were successfully achieved.

Measurements made during the demonstration included core maps of reaction rates, control rod worths, isothermal temperature coefficients, prompt neutron decay constants, and cycle-averaged fuel element powers and ^{235}U discharge burnups. Typical approach-to-critical measurements were also made for fresh HEU and LEU core configurations radially-reflected with both water and beryllium. In addition, uranium and plutonium isotopic mass ratios were measured as a function of ^{235}U burnup.

This report deals with a brief description of the ORR, a discussion of the experimental program conducted throughout the course of the whole-core LEU fuel demonstration, and, where possible, a comparison of measured results with analytical calculation

2. THE 30-MW OAK RIDGE RESEARCH REACTOR

2.1 Description of Facility

The Oak Ridge Research Reactor (ORR) is a 30-MW test reactor designed to accommodate a wide variety of irradiation experiments. With the reactor tank located in a deep pool of water, easy access with necessary shielding is provided from above the core.

The ORR is moderated and cooled with light water which is deionized to inhibit corrosion. It is fueled by 19-plate MTR-type fuel elements which are positioned by means of a rectangular grid plate with a lattice 9 elements wide and 7 elements long. The grid spacing is 3.035" x 3.189". Six shim rods, each with an upper cadmium poison section and a lower 15-plate fuel follower section, are used to control the reactor. To help provide easy access from the top, the control rod drive mechanisms are located below the core. The normal coolant flow rate for 30-MW operation is 18,000 gpm or 1.14 m^3/s. -

Normally the reactor is reflected radially with beryllium surrounded by a large pool of light water and axially with light water. The beryllium reflector elements have the same geometric cross section as the fuel elements and may be placed anywhere within the 9 x 7 grid array. A rectangular aluminum box surrounds the core and beryllium reflector.

Figure I shows a view of the ORR core and tank. The reactor first went critical in March 1958 and was shut down at the end of March 1987. Details concerning the ORR may be found in references (2) and (3).

2.2 Description of Fuel Elements

Standard fuel elements used in the ORR consist of 19 curved plates (13.97 cm. radius of curvature) as shown in Fig. 2. The highly enriched uranium (HEU) and the low-enriched uranium (LEU) fuel elements are of identical geometry but differ in fuel meat composition. Nominal dimensions of the fuel meat are 6.35 cm x 0.051 cm x 60.01 cm. with a cladding thickness of 0.038 cm. At the time of the demonstration fresh HEU elements contained 285 g ^{235}U in the form of a U308-Al dispersion and were fabricated by Texas Instruments (TI) and Babcock and Wilcox (B&W). On the other hand, the LEU elements contained 340 g ^{235}U in the form of a U_3Si_2-A1 dispersion and were fabricated by B&W, CERCA, and NUKEM with a uranium density in the fuel meat of 4.8 g/cc.

Table I shows the atom densities used in the diffusion calculations for fresh 19-plate fuel elements. These atom densities are homogenized over the fuel-clad-moderator portions of the fuel element but do not include the side plate regions beyond the width of the fuel meat. Absorbing effects of impurities and minor elements in the aluminum alloys are expressed in terms of an equivalent I (JB concentration.

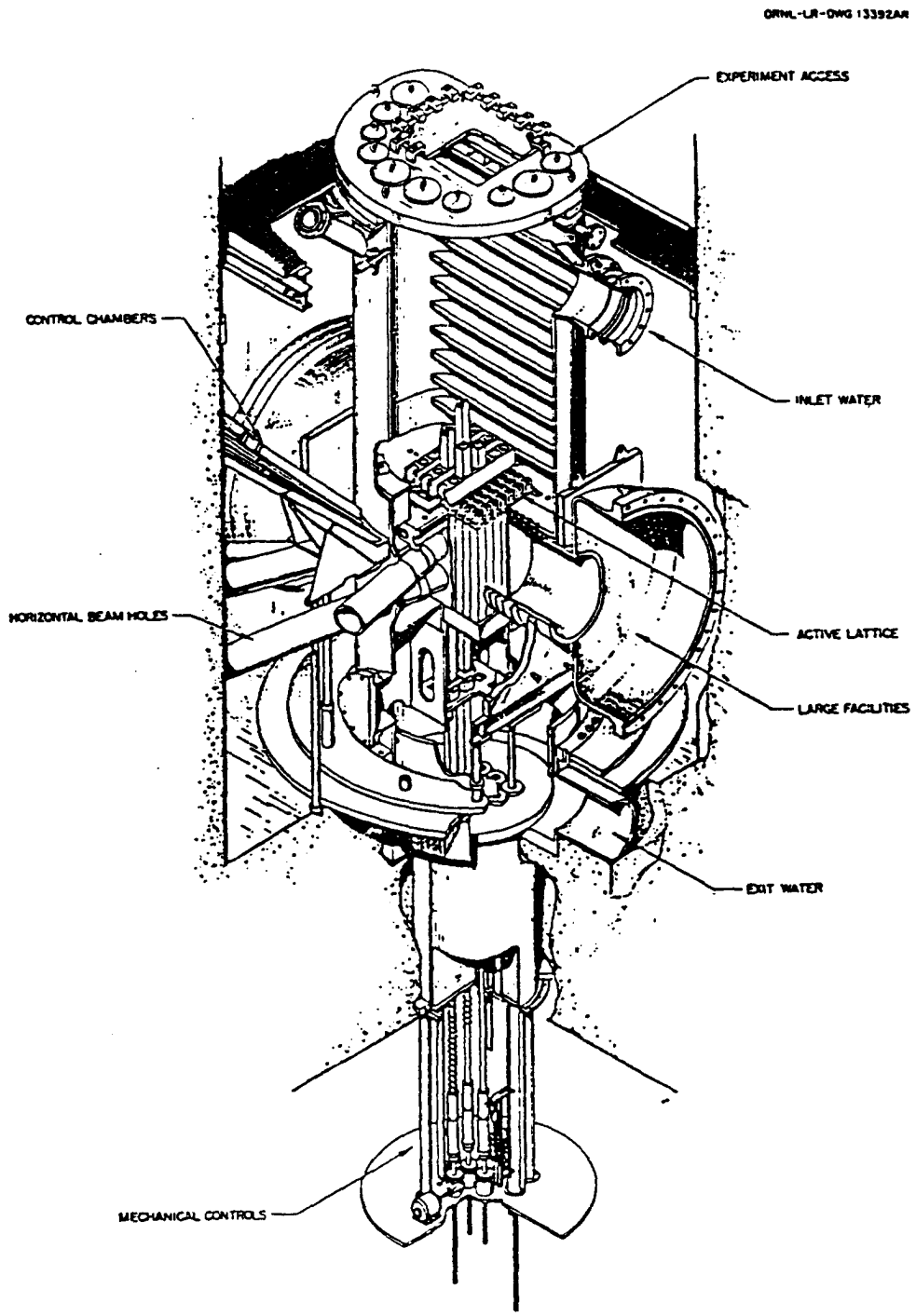

Fig. 1. View of the ORR Core and Tank

Dimensions in mm

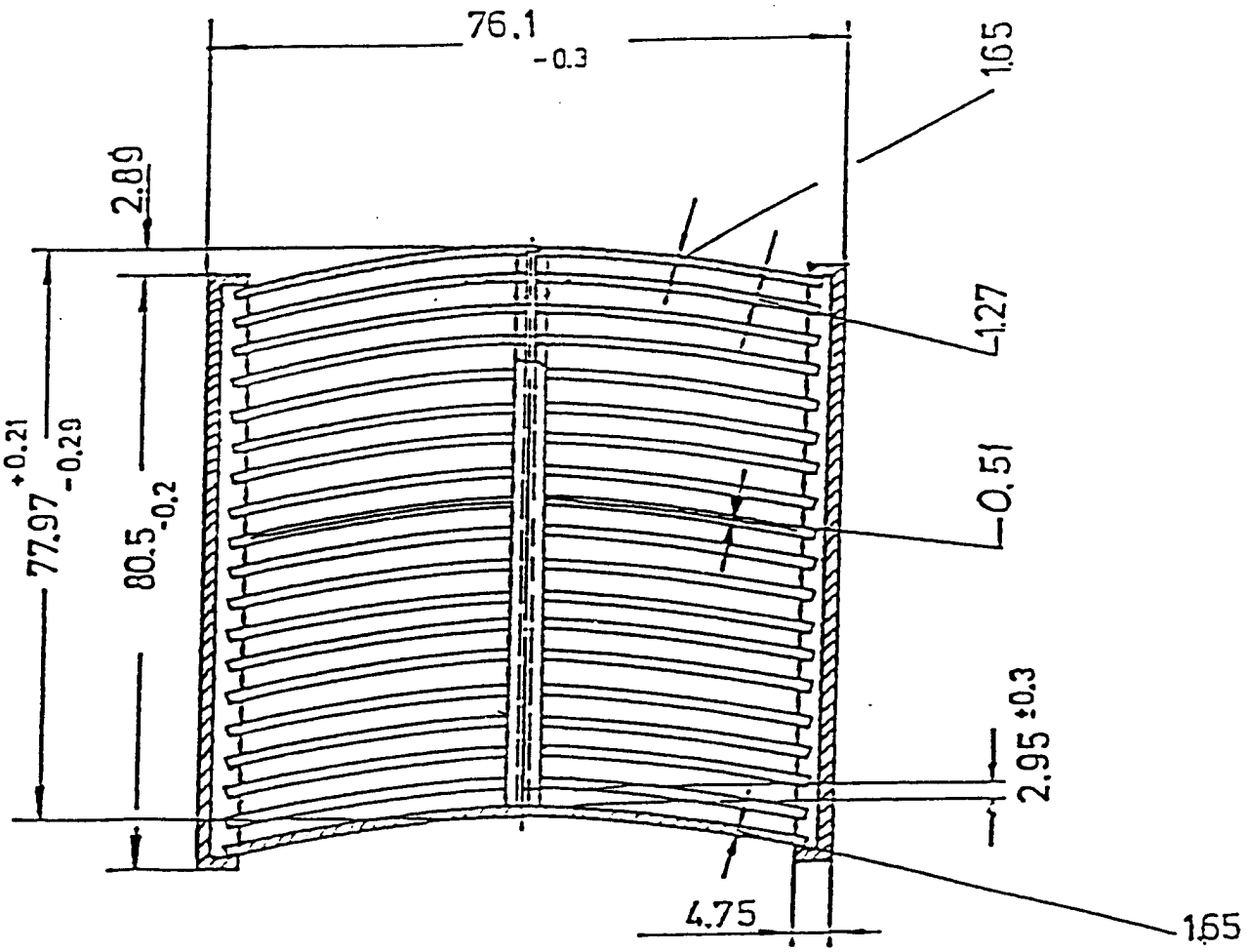

Fig. 2. Cross Section of Standard 19-Curved-Plate ORR Fuel Element

Table 1. Atom Densities Homogenized Over the Width of the Fuel Meat for Fresh 19-Plate Elements

Element/Isotope	Concentration in Atoms/barn-cm HEU Fuel	LEU Fuel
Hydrogen	4.6823E-02	4.6823E-02
Oxygen	2.4139E-02	2.3412E-02
Aluminum	1.6346E-02	1.4619E-02
Silicon		9.5410E-04
^{10}B (equivalent)	1.1227E-07	9.8601E-08
^{234}U	2.5833E-06	1.8819E-06
^{235}U	2.3936E-04	2.8555E-04
^{236}U	1.1080E-06	1.4353E-06
^{238}U	1.3747E-05	1.1380E-02

Table 2. Homogenized Atom Densities for the Fuel-Clad-Moderator Portion of Fresh 15-Plate Fuel Followers

Element/Isotope	Concentration in Atoms/barn-cm HEU Fuel	LEU Fuel
Hydrogen	4.6425E-02	4.6425E-02
Oxygen	2.3825E-02	2.3212E-02
Aluminum	1.6719E-02	1.5252E-02
Silicon		7.9640E-04
^{10}B (equivalent)	1.1452E-07	1.2502E-07
^{234}U	2.1479E-06	1.5708E-06
^{235}U	1.9902E-04	2.3836E-04
^{236}U	9.2122E-07	1.1981E-06
^{238}U	1.1430E-05	9.4991E-04

2.3 Description of Shim Rods

2.3.1 Poison Section

Shim rods used in the ORR consist of an upper cadmium poison section and a lower fuel follower section. The poison section is made of a 0.040-in.-thick sheet of cadmium clad on both sides with 0.020-in. aluminum. This composite sheet is formed into a hollow square annulus 2.345 in. on a side and 30.5 in. long. The cadmium box insert is contained within an aluminum shell whose outer dimensions are identical to those of the lower fuel follower section. The shell has a nominal thickness of 0.234 in. There is a 2-inch transition region between the top of the fuel follower plates and the bottom of the cadmium. In operation, the square annulus is filled with water.

2.3.2 Follower Section

The fuel follower section consists of 15 fuel plates each 0.127 cm thick with a meat thickness of 0.0508 cm. Two outer plates of curved solid aluminum form part of the outer housing. The fuel meat has approximately the same dimensions as that for the standard elements. Fresh fuel followers contain 167 g and 200 g ^{235}U for HEU and LEU fuel, respectively. Table 2 shows the homogenized atom densities for the fuel-clad-moderator portions of fresh fuel followers.

As for the standard 19-plate fuel elements, the HEU fuel meat in the followers consists of a $U_3 0_8$-Al dispersion and a U_3Si_2-A1 dispersion for the LEU followers. The LEU fuel followers were fabricated by Babcock and Wilcox with a uranium density in the fuel meat of 3.5 g/cc.

2.4 Beryllium Reflector Elements

The beryllium reflector elements are designed to fit into the grid lattice positions and so have the same cross sectional dimensions as the fuel elements (Fig. 2). Aluminum end boxes, similar to those used on the fuel elements, are fitted onto both ends of the beryllium block, whose overall length is 31.375 inches.

Two types of beryllium elements are used. One type, for use only as a reflector element, has a 3/16-in. coolant hole drilled longitudinally through the center of the block. The second type consists of a beryllium block with a 2-in. hole drilled through its center together with a 1-7/8-in. diameter plug of solid beryllium. With the insert this second type may be used in place of a standard beryllium reflector element. Without the insert and located either in a core or a reflector position the beryllium piece forms the outer portion of an isotope production facility.

2.5 Experimental Facilities Extraneous to Demonstration

2.5.1 Beam Tubes

Six horizontal beam tubes are located on the east side of the core. They each have an inside diameter of 6-7/8 in. at the reactor core box. When used as a beam facility, each beam tube is equipped with a collimator plug. When not in use the beam holes are shielded with plugs which seal the outer ends of the beam tubes. Figures 3 and 4 show the location of the beam holes with respect to the reactor and shield. Throughout the demonstration the beam tubes were plugged and voided. Both transport and Monte Carlo calculations showed that the perturbing influence on flux distributions within the core from neutron leakage through the beam tubes could be approximated in diffusion calculations by filling the beam tubes with water at 3% of normal density.

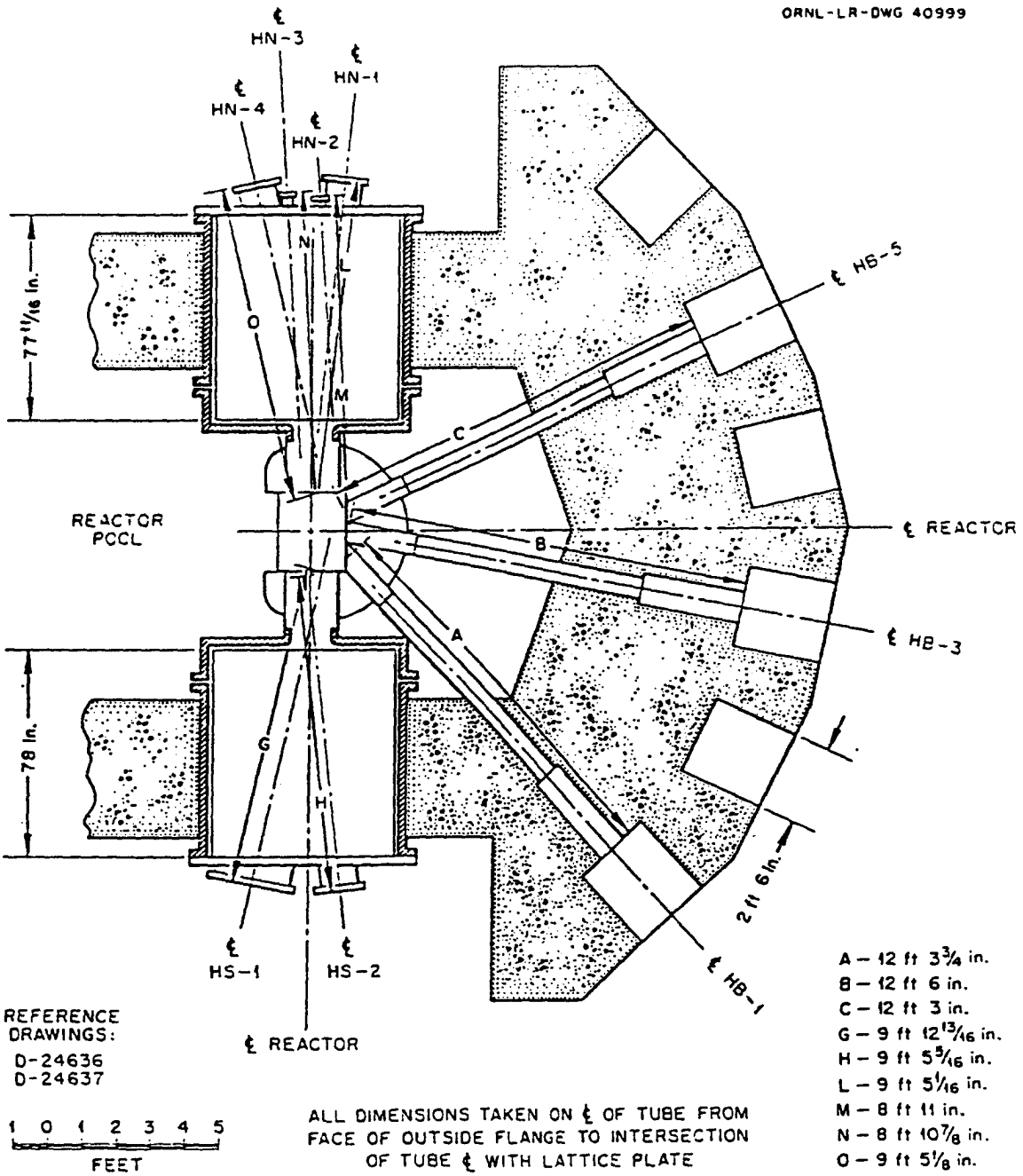

Fig. 3. Location of Beam Holes and Facility Plugs, Section 4-1/2 Inches Below Reactor Centerline

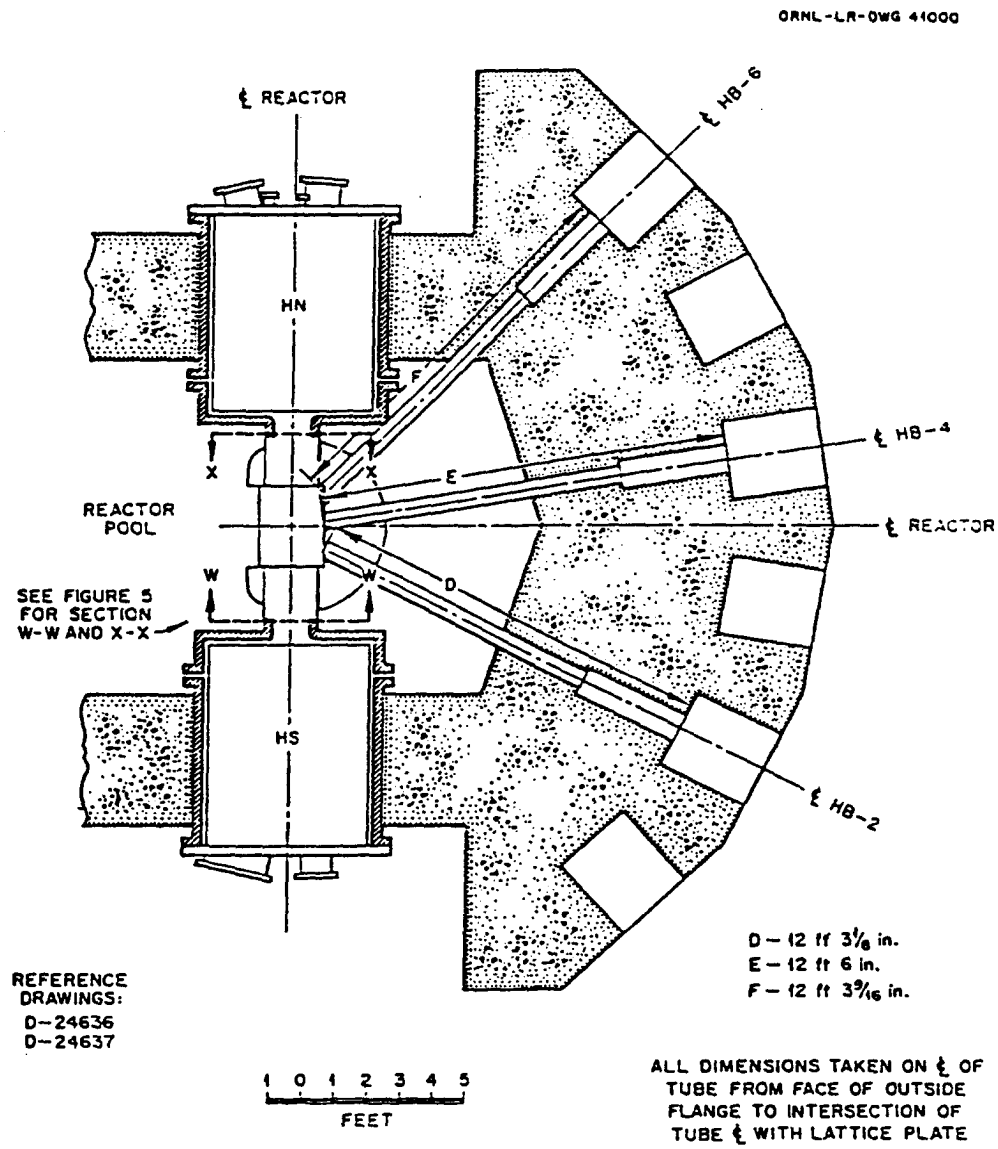

Fig. 4. **Location of Beam Holes and Facility Plugs, Section 4-1/2 Inches Above Reactor Centerline**

2.5.2 Engineering Facilities

On the north and south sides of the reactor large experiment rigs which require an appreciable volume close to the core can be accommodated. Obround holes, approximately 19 x 25 in. at the core face, are provided for this purpose. Shielding plugs are used to seal these holes when not in use. Throughout the demonstration no experiments were conducted which required the use of these engineering facilities. Because of large uncertainties about their contents, the engineering facilities were replaced with pool water in the reactor computations. Sketches of the engineering facilities are included in Figs. 3 and 4.

2.5.3 Heavy Section Steel Technology (HSST) Experiment

This experiment was designed to investigate fast neutron (A. 1 MeV) irradiation damage to pressure vessel components. The facility consists of a steel gamma ray shield approximately 8 cm thick followed by a pressure vessel simulator approximately 12.7 cm thick and is located in the reactor pool on the west side of the reactor tank. It is equipped with tracks and drive mechanisms which permit moving the HSST relative to the reactor face. Normally the HSST is withdrawn at reactor startup and then moved as close as possible to the flat west side of the reactor tank after equilibrium xenon concentrations prevail. Beginning with core 176A the HSST was fully withdrawn and no longer used in any of the remaining demonstration cores.

2.5.4 Europium and Iridium Isotope Production

Radioactive isotopes of europium and iridium are produced in the beryllium reflector and in the core, respectively. Samples of natural europiurn and iridium in the form of pellets (approximately 3/16-in. in diameter and 1/16-in. thick) am mounted on aluminum stringers and held in place by a close-fitting aluminum sleeve. These assemblies am placed into the hollow beryllium elements for irradiation and are sized to fit inside the hole and still provide a coolant gap around the outside.

2.5.5 Magnetic Fusion Experiments (MFE)

The magnetic fusion experiments were designed to measure neutron irradiation damage to materials proposed for first wall use in a magnetic fusion device. These experimental facilities are located within the core at grid positions C3 and C7. The experiment at C3 (NIFE-7J) contains a sodium-potassium alloy whereas that at C7 (NIFE-6J) does not. These MFE experiments were modeled using material volume fractions supplied by Oak Ridge.4

2.5.6 High Uranium-Loaded Fuel Element Development (HFED) Facility

The HFED5 was designed for the irradiation-testing of miniature fuel plates (miniplates) of various compositions and densities in the ORR at core position E3. These miniplates were 114 min long, 50 wide, and either 1.27 mm or 1.52 mm thick with a 0.20-mm minimum cladding requirement. They were loaded into an irradiation device containing five stacked modules. When assembled, the HFED resembled an ORR element with narrow fuel plates. Results from many of these miniplate irradiations, with particular emphasis on the U3Si2-Al dispersion fuels, are given in Ref. 6.

Figure 5 shows a core map for one of the HEU/LEU mixed cores. Note the presence of the various experimental facilities. The pressure vessel simulator and the gamma shield form part of the HSST experiment. Miniplates are irradiated in the HFED assembly. The engineering facilities are not shown in this figure but are located on the north and south sides of the core. The east direction is at the bottom of the figure, where the beam tubes emerge from the core box.

ORR CORE MAP FOR CYCLE 175C

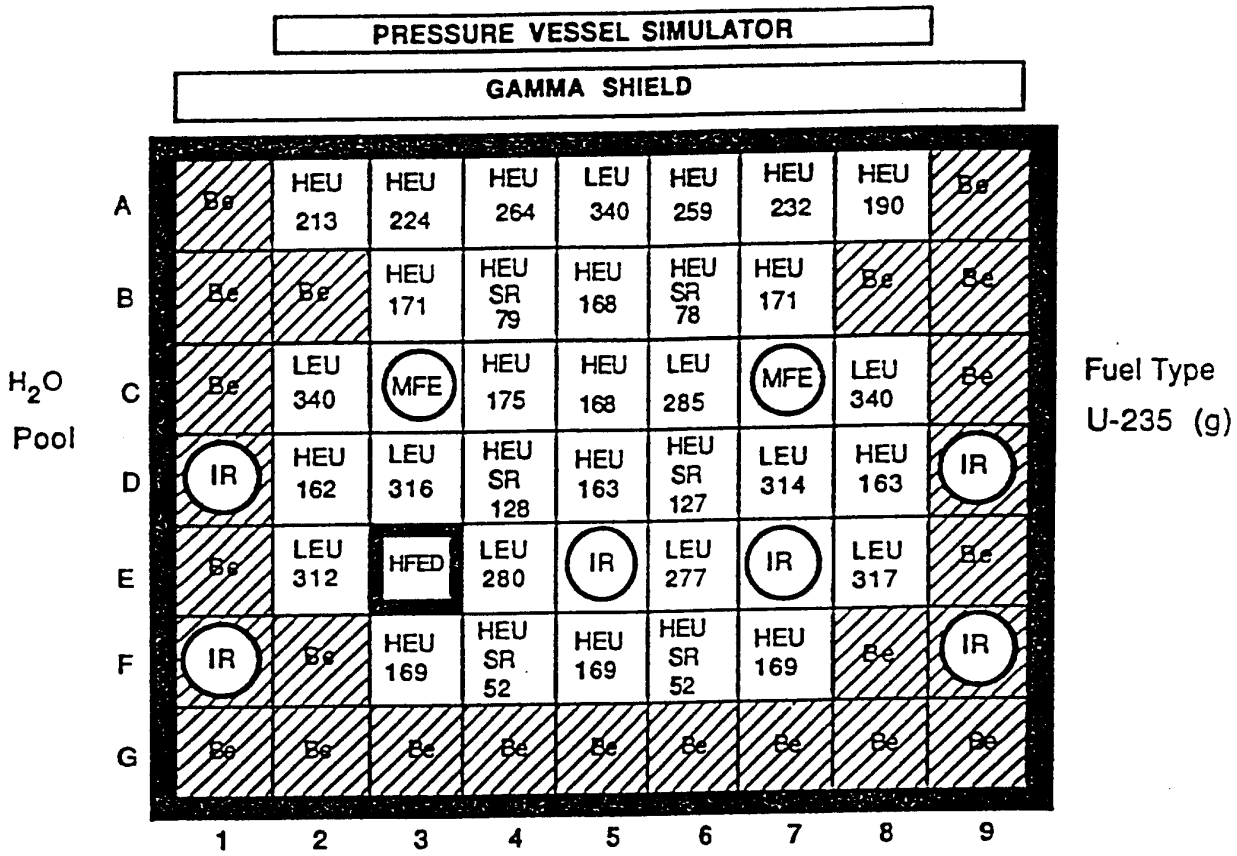

SR ≡ Shim Rod assemblies

MFE ≡ Magnetic Fusion Experiment

HFED ≡ High uranium density Fuel Element Development

IR ≡ Irradiation facility for activating iridium or europium samples

Six voided beam tubes (17.46 cm ID) exit the core box on the bottom side of the figure.

Fig. 5

3. **SAFETY EVALUATIONS**[7]

Major issues addressed in the safety assessment of the whole-core demonstration in the ORR were the irradiation performance of the fuel, fission-product release and radiological consequences, minimum margin to burnout, and transient response. Except for fuel performance, these issues were addressed on a relative basis, comparing the behavior of the LEU and mixed LEU/HEU transition cores to that of a typical HEU core. Brief descriptions of some of the analyses are presented in this section.

The assessment of the irradiation performance characteristics of the U3Si2 fuel was based upon the very good results obtained during the tests of four miniature fuel plates (at 3.75 g U/cc) and six full-sized fuel elements identical to those used in the demonstration (4.8 gU/cc). Two test elements were fabricated by each of the three fabricators from which the fuel elements for the demonstration were subsequently ordered. The irradiation tests covered the full range of burnups expected in the fuel elements and shim rod followers. The results of the element irradiations are discussed elsewhere. I

The assessment of the relative severity of the radiological consequences for the LEU core versus the HEU core following an accident postulated to release a given fraction of available fission products and plutonium was based upon a generic assessment performed by Woodruff.[8] Although the generic analysis assumed the release of 1% of the plutonium contained in a fuel clement and showed that the plutonium dose was not the limiting factor, there appears to be no credible mechanism for release of any plutonium during the types of accidents which the ORR could hypothetically experience.

Neutronics data for the margin-to-burnout and transient analyses were obtained from three-dimensional diffusion-theory calculations of the HEU, LEU, and transition cores, using standard RERTR methods and codes. Fuel cycle calculations for a core containing 28 fuel elements and six shim rods were performed to obtain fuel loading distributions for subsequent use in more-detailed stand-alone calculations to obtain values of safety-related parameters. The fuel cycle calculations were performed with four of the shim rods banked at their estimated middle-of-cycle position (two shim rods are normally fully withdrawn during ORR operation) in order to obtain approximately the correct axial burnup distribution. What is believed to be a worst-case arrangement of experiments in the core (in terms of power distribution) was used. Some results from the equilibrium core calculations are listed in Table 3. Power distributions for the margin-to-burnout and transient analyses were determined for startup conditions, i.e., beginning-of-cycle fuel loadings were used, the core was Xe free, all previously irradiated elements contained saturated Sm concentrations, and the four banked shim rods were inserted halfway.

The margin-to-burnout, with critical heat fluxes calculated using the Labuntsov correlation, has traditionally been used to access the steady-state thermal-hydraulic safety of the ORR. An extensive assessment of the minimum margins to burnout was performed for the HEU, LEU, and transition cores. Margins were calculated both on the basis of core power ($Mq^{P,F}$) and heat flux ($MQ^{P,F}$) for various power (P) and flow (F) conditions. Core powers used in the analysis were the normal operating power (30 MW) and the limiting safety system setting for power (47 MW). Total core flow rates used were the normal operating flow rate (1.17 m^3/s), the flow-rate limiting safety system setting (0.85 m^3/s), and an intermediate flow rate (0.96 m^3/s). A considerable number of conservatisms were used in the calculations to account for possibilities allowed by the fuel specifications or for uncertainties in measured and calculated quantities. Some of the results of these calculations are listed in Table 4. It is seen that the minimum margin for limiting power and flow conditions occurs at the bottom of the fuel element. The LEU and HEU cores are comparable, but a somewhat larger power peak in the transition core results in a reduced margin.

Table 3. Comparison of Basic Equilibrium Cycle Parameters for 285-g HEU and 340-g LEU ORR Cores.

Parameter	285-iz HEU Core	340-K LEU Core
Banked Shim Rod Position, cm (in.) withdrawn	56.665 (22.305)	58.415(22.998)
k_{eff} (BOEC)[a]	1.0502	1.0435
k_{eff} (MOEC)[a]	1.0152	1.0160
k_{eff} (EOEC)[a]	0.9853	0.9941
k_{eff} (EOEC)[b]	1.0174	1.0152
$\Delta\rho$/full power day,[c] $\%\Delta k/k$/fpd	-0.299	-0.181
^{235}U (BOEC), kg	6.247	7.644
^{235}U (EOEC), kg	5.491	6.799
Cycle length, fpd	20.0	24.0
Core ^{235}U Burnup, g/MWd	1.26	1.17
Ave. Discharge ^{235}U Burnup of Standard Element, %	59.9	55.9
Ave. Discharge ^{235}U Burnup of Shim Follower, %	81.4	79.9
Control Rod Worth (BOEC) All Rods, $\%\Delta k/k$	-26.25	-25.05

[a]BOEC, MOEC, EOEC: Beginning, middle, and end of equilibrium cycle.
[b]With all shim rods fully withdrawn.
[c]Based upon reactivity change from MOEC to EOEC.

Table 4. Margins to Burnout in Limiting Channel of Standard Fuel Element in Hottest Core Position

Core	X[a], *m*	q^{30}_{max} *MW/M*^{2}	$M_q^{30,1.17}$	$M_Q^{30,1.17}$	q^{47}_{max} *MW/M* ^{2}	$M_q^{47,0.96}$	$M_Q^{47,0.96}$	$M_q^{47,0.85}$	$M_Q^{47,0.85}$
HEU	0.613	1.91	4.69	2.67	2.99			1.81	1.33
HEU	0.542	2.00	4.73	2.87	3.13			1.94	1.43
HEU	0.486	2.28	4.33	2.92	3.57			1.87	1.46
HEU	0.365	2.39	4.52	3.48	3.74			2.15	1.77
LEU	0.613	1.94	4.59	2.63	3.04			1.75	1.31
LEU	0.489	2.25	4.36	2.90	3.53			1.86	1.45
LEU	0.433	2.39	4.29	3.07	3.75			1.93	1.55
LEU	0.368	2.43	4.42	3.41	3.81			2.09	1.73
TRN[b]	0.613	2.09	4.18	2.44	3.27	1.79	1.34	1.53	1.22
TRN	0.542	2.19	4.24	2.63	3.42	1.92	1.44	1.67	1.31
TRN	0.486	2.49	3.90	2.67	3.90	1.85	1.47	1.63	1.34
TRN	0.365	2.61	4.09	3.19	4.10	2.11	1.76	1.92	1.62

[a]Distance below top of fuel. The bottom of the core is at x = 0.613 m; the peak heat flux occurs at x = 0.37 m.
[b]Transition Core

The margins during the transition can be maintained at the levels of those for the HEU core by raising the low-flow-rate safety system setting.

Analyses of the response of the ORR to reactivity insertions were calculated using the ANL-modified version of the PARET code.9 Both startup (rod withdrawal) and rapid reactivity insertion accidents were studied. Basically the same conservatisms were applied in the transient analyses as were applied in the margin-to-burnout analyses, since the relative responses of the system studied would be quite insensitive to the choice of conservatisms. No representation is made that this choice of conservatisms is proper for any but relative comparisons. The basic input parameters for the calculations are shown in Table 5, and the results of the rapid reactivity insertion analyses are given in Table 6. In all cases the LEU core is able to withstand a larger step insertion than the HEU core before clad melting begins. The transition core was modeled as an HEU core with LEU fuel meat properties and transition core power peaking factors. Therefore, it could accommodate slightly smaller step insertions than the HEU core. However, the differences are sufficiently small considering the conservative (HEU) kinetics and reactivity feedback assumptions.

Table 5. Parameters for ORR Transient Analyses

Selected Parameter	HEU	LEU
Neutron Generation Time, μs	71.19	60.48
Effective Delayed Neutron Fraction, %	0.7444	0.7132
Temperature Coefficients, $/°C		
Water Temperature Only	1.991-02	1.545-02
Fuel Temperature	8.295-05	3.253-03
Coolant Void Coefficient, $/% Void	1.713-01	2.292-01
Fuel Thermal Conductivity, W/m K	175.0	130.0
Fuel Heat Capacity, (J/m^3 K)	2.420+06	2.150+06 + 1.100+03 *T
Cladding Thermal Conductivity, W/m K	180.0	130.0
Cladding Heat Capacity, J/m^3 K	2.427+06	2.427+06
Rod Worths, $		
B4, B6, D4, and D6	27.834	26.827
F4 and F6	4.002	4.131
Rod Withdrawal Rate, mm/s	2.12	2.12
Rod Scram Acceleration (relative to g)	0.6	0.6

Table 6. Comparison of the Response of the ORR to a Rapid Reactivity Step Insertion for HEU, LEU, and Transition Cores.
(Hot channel in standard fuel element; maximum differential rod worth)

Core	Init. Power (MW)	Power Trip Level (MW)	cool. Flow Rate (m/S)	Inlet Temp. (°C)	Init. React. ($)	React. After Step ($)	Min. Period (ms)	Max. Power (MW)	Max. Fuel Temp. (°C)	Max. Clad. Temp. (°C)
HEU	10^{-6}	0.966	0.305	35.0	-1.0	1.90	3.3	336	589	583
LEU	10^{-6}	0.966	0.305	35.0	-1.0	1.90	3.0	356	568	562
TRN	10^{-6}	0.966	0.305	35.0	-1.0	1.85	3.4	240	568	563
HEU	10^{-6}	43.5	8.17	35.0	-1.0	1.50	3.9	341	564	551
LEU	10^{-6}	43.5	8.17	35.0	-1.0	1.70	3.2	435	566	491
TRN	10^{-6}	43.5	8.17	35.0	-1.0	1.45	4.0	289	514	467
HEU	30	43.5	8.17	49.9	0.0	1.25	7.7	279	491	467
LEU	30	43.5	8.17	49.9	0.0	1.40	6.1	326	512	488
TRN	30	43.5	8.17	49.9	0.0	1.20	8.0	254	558	519

4. THE EXPERIMENTAL PROGRAM

4.1 Introduction

The experimental program was designed with four primary objectives in mind:

I To demonstrate the acceptable performance of commercially- fabricated LEU U_3Si_2-Al fuel elements to average ^{235}U burnups greater than 50%,

2. To provide a wide base of experimental data for testing analytical methods and codes,

3. To obtain information necessary to verify that required safety margins were maintained for all the cores used in the demonstration, and

4. To demonstrate the safe and acceptable reactor performance throughout the gradual transition from an all-HEU near-equilibrium core, through a series of mixed HEU/LEU cores, to an all-LEU near-equilibrium core.

To allow for xenon decay, the ORR operates with a two-core fuel management system. After each cycle all the fuel elements (except the six shim rod fuel followers) are removed from the core and stored in the pool. Fuel elements from the previous core are loaded back into the reactor in preparation for the next cycle. During this transition three (or four) unirradiated LEU elements are loaded on the outer edge of the core, three (or four) spent HEU elements are removed from central core positions, and the remaining elements are redistributed throughout the core. Normally, fresh shim rods are loaded into positions D4 and D6 after four successive operating cycles. Those in D4 and D6 are moved to B4 and B6 and those in B4 and B6 are relocated into the F4 and F6 positions. Spent control rods are removed from positions F4 and F6 and moved to pool storage. After having been in the reactor for about nine months of operation the spent shim rods achieve an average discharge burnup of about 75%.

4.2 Low Power Measurements

4.2.1 Reaction Rate Distributions

^{60}Co and ^{198}Au activity distributions have been measured throughout a number of cores by means of wire activation techniques. Normally, 0.020-inch diameter cobalt-vanadium wires (2.0 wt% Co) are used for this purpose. Co-V wires are inserted axially into water channels between fuel plates using aluminum holders of the type shown in Fig. 6. The wires extend approximately one inch above and below the active fuel region. Each fuel element in the core is monitored with at least two Co-V wires. Additional wires are loaded into those fuel elements expected to have the highest power densities. An underwater TV camera is used to ensure the proper location and alignment of the monitors in the fuel elements. A 0.080-inch diameter aluminum tube is used to position wires in the fuel followers. However, the shim rod geometry makes the precise location and alignment of these wires uncertain. A similar arrangement is sometimes used to position wires in the beryllium reflector elements.

All the Co-V wires are irradiated simultaneously for six hours at a power level of approximately 300 kW. The axial distribution of the ^{60}Co activity is measured by means of a computer-controlled wire-scanning system. A discriminator window is set on the output signal from a NaI detector so that only the two ^{60}Co photopeaks are recorded. A typical profile of the ^{60}Co activity is shown at the bottom of Fig. 6. This distribution shows the flux peaking which occurs in the axial reflectors.

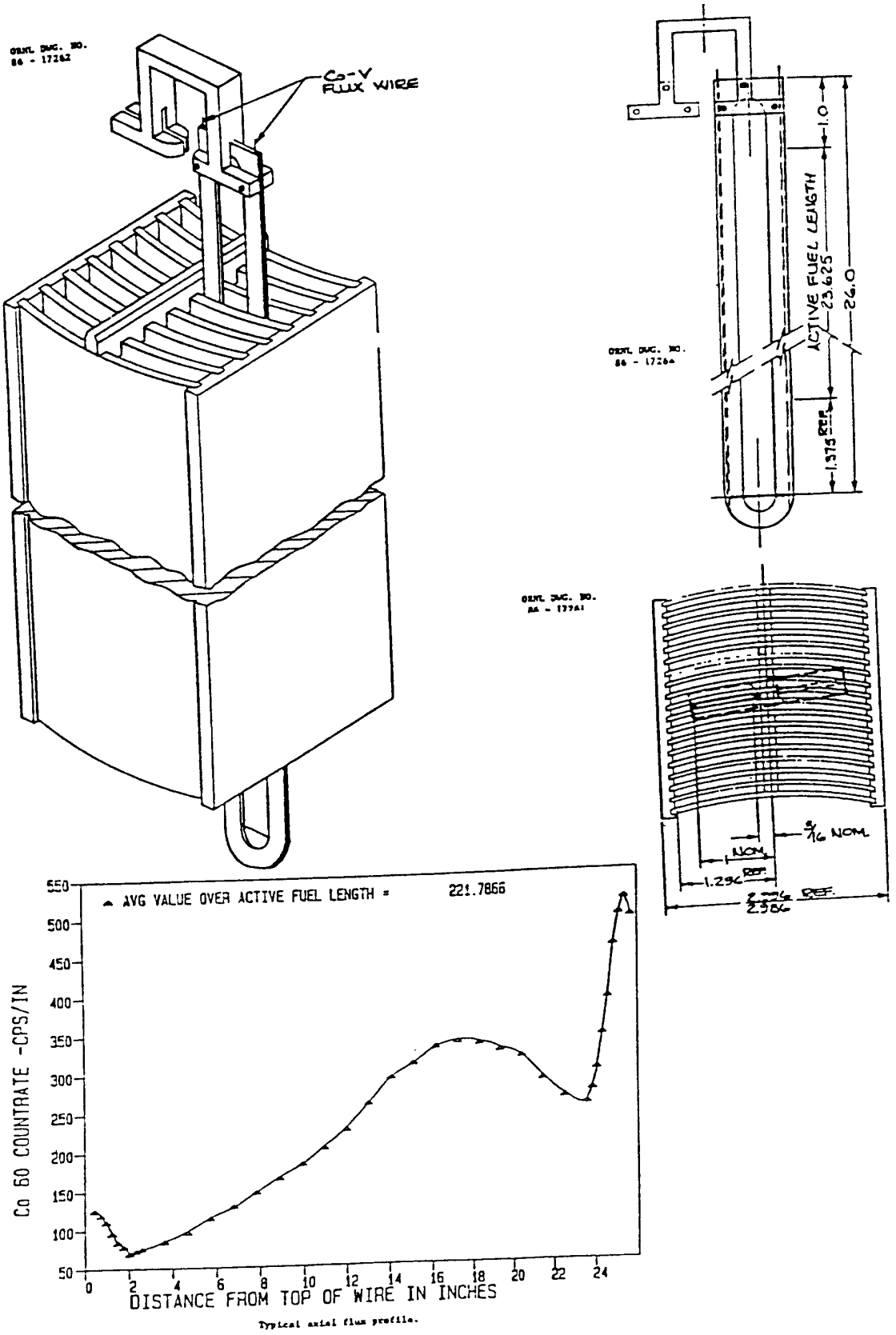

Fig. 6. Aluminum Holders for Cobalt-Vanadium Wires

The wire activation data may be used to determine power density peaking factors, fuel element powers, and activation distributions throughout the core which may be compared with calculations. Neutron flux gradients, determined by comparing activities of multiple wires activated in the same fuel element are used to determine power density peaking factors. Combining this information with all the wire data allows a determination of the total peak -to- average power density. This information was used to deter-mine the maximum heat flux (luring full power operation and the safety margin defined as the ratio of the critical heat flux to the maximum heat flux at the limiting conditions chosen for ORR operation during the demonstration (43.5 MW and 14,100 gpm flow). At this limiting condition the minimum allowed safety margin is 1.6 (see Ref. 10). Safety margins based on Co activation data, which were used to obtain required approvals prior to operation at full power for cores 174C, 175A, 176B and 177B, are shown in Table 7 (see Ref. 11). For comparison, safety margins based on calculated total peak-to-average power densities are included in this table.

The power produced in a fuel element is assumed to be proportional to the product of the ^{235}U fuel element mass and the axially- averaged 60Co activity for wires closest to the center of the element. By normalizing the sum of the above products to the total reactor power, fuel element powers can be determined.

A comparison of measured 60Co activity distributions throughout reactor cores with calculated values is given in Section 7.2 of this report. Core flux mapping based on gold wire activations was obtained only for the water-reflected cores containing all fresh HEU and all fresh LEU fuel. To minimize fuel activation, these cores were operated at powers well below 300 M Therefore, gold rather than Co-V wires had to be used in order to get adequate counting statistics. Results from these measurements are also discussed in Section 7.2.

4.2.2 Control Rod Worths

An operating requirement for the ORR is that the reactor remain subcritical with all the shim rods withdrawn approximately halfway. This condition was met for all the cores used in the demonstration.

Control rods were calibrated periodically throughout the demonstration using the positive period method. The measurements were made as follows. One of the six control rods was fully inserted while the remaining five rods were ganged together and moved to achieve criticality. The first rod was then withdrawn a small measured amount, the positive period measured, and the differential rod worth determined at this position. This rod was then withdrawn about 2 inches from the "on-seat" position and the others ganged to critical. Another differential worth measurement was made at this location. This process was repeated until the limit of rod travel was reached. The total rod worth was obtained by integrating the differential worths from the lower to the upper limit of rod travel. This procedure was repeated for each of the remaining five rods.

In general, poor agreement was obtained between calculated and measured differential and integral rod worths. Toward the end of the demonstration it was found that negative temperature-related feedback effects contaminated the asymptotic period measurements and that delayed neutron parameters used to convert periods to reactivities had to include contributions from delayed photoneutrons. Reasonable agreements with calculations were obtained when differential worths were determined from the initial shape of the measured flux profile following the positive reactivity insertion. These matters are discussed more fully in Sections 6.2 and 7.3 of this report.

For each operating cycle a history of the control rod positions at critical versus time was recorded. This information was used in the burnup calculations which allowed for shim rod movement during the burn cycle (see Appendix B).

Table 7. ORR DNB* Safety Margins at Normal Operating Conditions

	Configuration				Core	Safety Margin	
	Fuel Elements		Fuel Followers		Position	Wire Data	Calc.
Core	HEU	LEU	HEU	LEU			
174C	27	0	6	0	C6	2.12	2.00
174FX	20	7	6	0	D7	2.52	
175A	20	7	6	0	D3		1.95
176AX1	13	14	4	2	E4	2.13	
176B	13	14	4	2	C4		1.82
177AX1	4	21	2	4	E4	1.87	
177B	4	21	2	4	D4		2.05
179A	0	27	0	6	D6		1.86

*DNB = departure from nucleate boiling

4.2.3 Prompt Neutron Decay Constant

Reactor noise analysis techniques12 were used to measure the prompt neutron decay constant in several cores. The prompt neutron decay constant is just the ratio of the effective delayed neutron fraction to the prompt neutron lifetime. Signals from two fission chambers located on opposite sides of the core and near the core midplane were processed by a Fourier analyzer to obtain the cross power spectral density (CPSD) as a function of frequency. This frequency spectrum was analyzed by least-squares techniques to obtain the break frequency, which when multiplied by 2Tc gives the prompt neutron decay constant. These measurements are straightforward in principle, but need to be made at very low power. In partially burned cores the measurement is difficult because of relatively strong neutron backgrounds from both spontaneous fission and photoneutron production. Results of these measurements are discussed in Section 7.4 of this report.

4.2.4 Critical Assemblies with Fresh Fuel

A number of critical cores radially reflected with either beryllium or water were assembled using unirradiated HEU and LEU fuel elements and fuel followers. These measurements provided a set of simple benchmark data which were used to test reactor codes and modeling methods. Results of these tests are discussed in Section 7.1 of this report.

Measurements made in these cores included:

1. Approach-to-critical determinations

2. Shim rod calibrations

3. Core mapping of ^{198}Au activities obtained from irradiated Au wires

4. Determinations of the prompt neutron decay constant

The last two measurements were made only in the water-reflected cores.

4.2.5 Isothermal Temperature Coefficient

The isothermal temperature coefficient was measured in an all-LEU core near the end of the demonstration. With the water coolant at its lowest temperature, shim rods F4 and F6 were withdrawn to their upper limits, D4, D6 and B6 were banked together at a fixed position approximately halfway withdrawn, and B4 was slowly withdrawn to achieve criticality. The coolant temperature slowly increased because of friction heating in the cooling system. With about every 30C rise in temperature the B4 critical rod position was redetermined. This measurement process was repeated over a temperature range from 25 to 450C. In addition, the differential worth of the B4 shim rod was measured over the same rod displacement interval. Since temperature changes occurred very slowly and because the reactor was subcritical most of the time, this measurement was made under isothermal conditions. Results of these measurements are discussed in Section 7.5 of this report.

4.2.6 Reactivity Worths of Experimental Facilities

A number of experimental facilities were present in the ORR during the whole-core demonstration even though they did not contribute directly to the objectives of the demonstration. The neutronics calculations had to take these experiments into account. To check how adequately these experimental facilities were modeled in the calculations, a number of reactivity substitution measurements were made. Changes in critical rod positions were determined when the MFE's, the HSST, the HFED, and the Eu and Ir isotope production facilities were individually replaced with water and, in some cases, with solid aluminum elements. Most of these substitution measurements were made at the start of the demonstration in the all-HEU core 174C.

Because of the fast neutron threshold reaction 9Be(n, (X)6He, 6Li and 3He poisons build up in the beryllium reflector elements. To check how well the model accounts for these poisons, the worths of several beryllium reflector elements were measured relative to an unirradiated beryllium element.

In general, reactivity substitution measurements verified that the experimental facilities were adequately modeled in the neutronics calculations. Some results are shown in Section 5.8.4 of this report.

4.3 Full Power Cores

Some characteristics of the twenty-two 30-MW operating cores used in the LEU fuel demonstration are given in Table 8. Core configurations, fuel element locations, and BOC ^{235}U fuel element masses may be found in Appendix A for each of these cores. Experimentally determined shim rod positions corresponding to criticality at various stages throughout the bum cycle are summarized in Appendix B.

The demonstration began with the all-HEU reference core 174C, which contained 27 fuel elements, 6 fuel followers, and operated for 16.84 full power (30-MW) days. After a series of mixed HEU/LEU cores, the first core to operate with all-LEU fuel was 178C. The last core to operate at full power before the final shutdown of the ORR was 179A.

4.4 Gamma-Scanning of Irradiated Full-Sized Fuel Elements

After each cycle of operation during the whole-core LEU demonstration, fuel elements from the ORR were removed from the core to allow for xenon decay while the next core was loaded with different fuel elements. During these intercycle periods each removed fuel element was gamma-scanned along the centerline to measure the axial distribution of the ^{140}La fission product activity. Because of the relatively short half lives involved, this information was used to determine fuel element powers and burnups which occurred during the previous operating cycle. In addition, discharged fuel elements were gamma-scanned for the ^{137}Cs fission product activity. Since ^{137}Cs has a 30-year half life, this measurement integrates the activity over all previous operating cycles and so gives information regarding the ^{235}U mass and burnup in the discharged fuel element.

Figure 7 shows a schematic diagram of the fuel element gamma-scanning apparatus[13] which is anchored at the edge of the reactor pool. The fuel element is placed horizontally in a tray located at the bottom of the pool. Under computer control, the element is moved beneath an air-filled vertical aluminum tube 1/2-inch in diameter to each of 16 predetermined counting locations along the element axis. The tube extends upward through about 16 feet of water to a lead collimator one foot long with a 1/16-inch diameter hole. Gamma rays are detected in a lithium-drifted germanium crystal (58 cm^3). Results from a gamma peak fitting routine for each axial location scanned are stored on floppy disks.

Table. 8 Summary of Operating Cores Used in the ORR Demonstration

CORE	HEU	LEU	Cycle Length[b]
174C	27+6	0+0	16.840
174D	24+6	3+0	12.855
174E	24+6	3+0	10.623
174F	24+6	3+0	15.428
175A	20+6	7+0	18.518
175B	20+6	7+0	20.305
175C	17+6	10+0	17.389
176A	17+6	10+0	17.244
176B	13+4	14+2	21.864
176C	14+4	14+2	19.436
176D	8+4	17+2	19.446
177A	8+4	17+2	14.773
177B	4+2	21+4	18.516
177C	4+2	21+4	18.411
177D	0+2	24+4	15.334
178A	0+2	24+4	12.101
178B	0+2	25+4	0.644
178C	0+0	26+6	11.138
178D	0+0	26+6	16.356
178H	0+0	26+6	20.277
178J	0+0	26+6	16.502
179A	0+0	26+6	20.169

[a]27+6 means 27 19-plate fuel elements and 6 15-plate fuel followers.
[b]Cycle length in full power (30 MW) days.

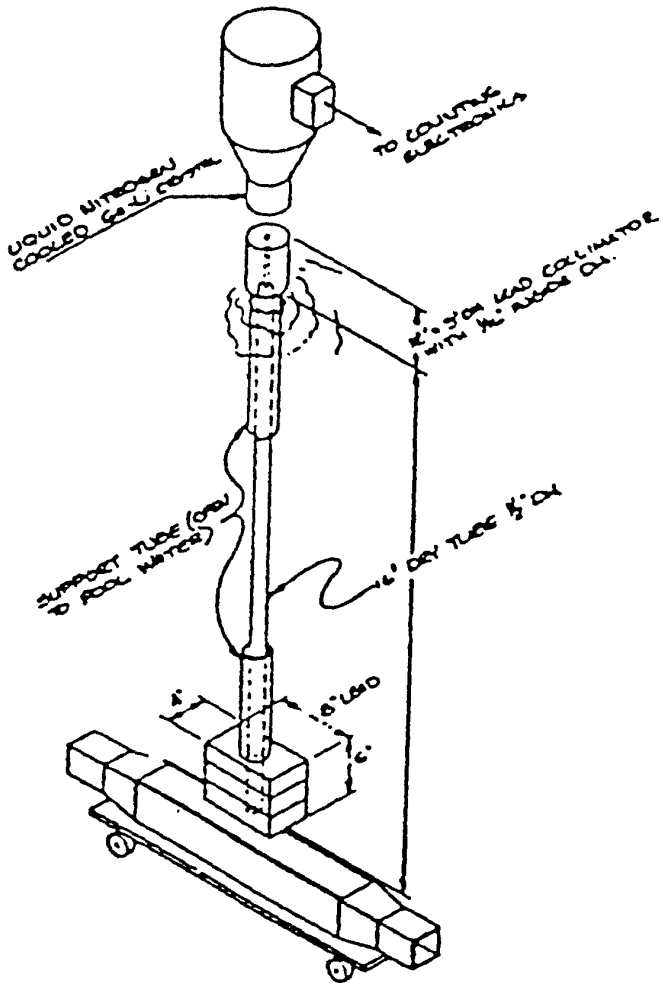

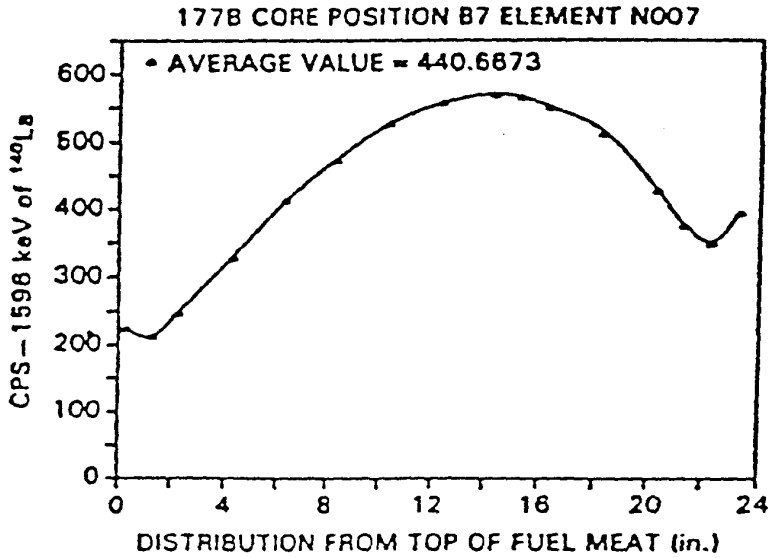

Fig. 7. Fuel Element Gamma-Scanning Apparatus

The fission product chains which lead to the production of ^{140}La and ^{137}Cs are

$$^{140}\mathrm{I}(0.86\mathrm{s}) \rightarrow {}^{140}\mathrm{Xe}(13.6\mathrm{s}) \rightarrow {}^{140}\mathrm{Cs}(63.76\mathrm{s}) \rightarrow {}^{140}\mathrm{Ba}(12.79\mathrm{d}) \rightarrow {}^{140}\mathrm{La}(40.3\mathrm{h}) \rightarrow {}^{140}\mathrm{Ce}(\mathrm{stable})$$

$$^{137}\mathrm{Te}(4\mathrm{s}) \rightarrow {}^{137}\mathrm{I}(24.5\mathrm{s}) \rightarrow {}^{137}\mathrm{Xe}(3.84\mathrm{m}) \rightarrow {}^{137}\mathrm{Cs}(30.17\mathrm{y}) \rightarrow {}^{137}\mathrm{Ba}(\mathrm{stable})$$

with cumulative fission yields of 6.28% and 6.22%, respectively. For ^{140}La, the gamma ray yield is 95.6% for the 1596 keV line. In the case of ^{137}Cs the 662 keV gamma ray has a yield of 84.6%. These are the gamma rays used in the gamma-scanning analysis system. Because of interfering gamma rays, the ^{137}CS scans cannot be recorded until most of the short-lived fission product activities have decayed away. About a three-month period is needed to allow for the decay of these interfering gamma rays. Figure 8 shows a measured gamma spectrum of an irradiated LEU fuel element measured with the Ge(Li) detector shortly after the element was removed from the core.

Near the end of the demonstration the Ge(Li) detector failed so that the remaining LEU fuel followers were gamma-scanned for ^{137}Cs using a standard 3" x 3" NaI detector. Special methods had to be developed to interpret this data.

Methods used to analyze the gamma-scanning data are discussed in Section 6.4 while results based on these analyses are presented in Sections 7.7 and 7.8.

4.5 ^{137}Cs Gamma-Scanning and Mass Spectrometry of Irradiated Fuel Plates

A number of selected fuel elements and fuel followers were disassembled following irradiation in order to perform postirradiation measurements on certain fuel plates. These measurements included ^{137}Cs gamma scans of individual fuel plates in both the longitudinal and transverse directions using a 3.18-mm-diameter collimator and a Ge(Li) detector. In addition, samples for mass spectrometric analyses were cut from some of these plates.

These data were used to make an independent determination of fuel-element- averaged ^{235}U burnups. Pointwise burnups were obtained from the measured uranium mass spectra while the gamma-scanning data allowed these point values to be converted to burnups averaged over the whole fuel element. In addition, uranium and plutonium isotopic ratios were measured as a function of burnup. Also, isotopic dilution methods were used to determine burnup-dependent values for the uranium and plutonium content per gram of fuel meat.

Methods used to analyze these data are discussed in Section 6.5 of this report while results are given in Sections 7.8.2 and 7.9.

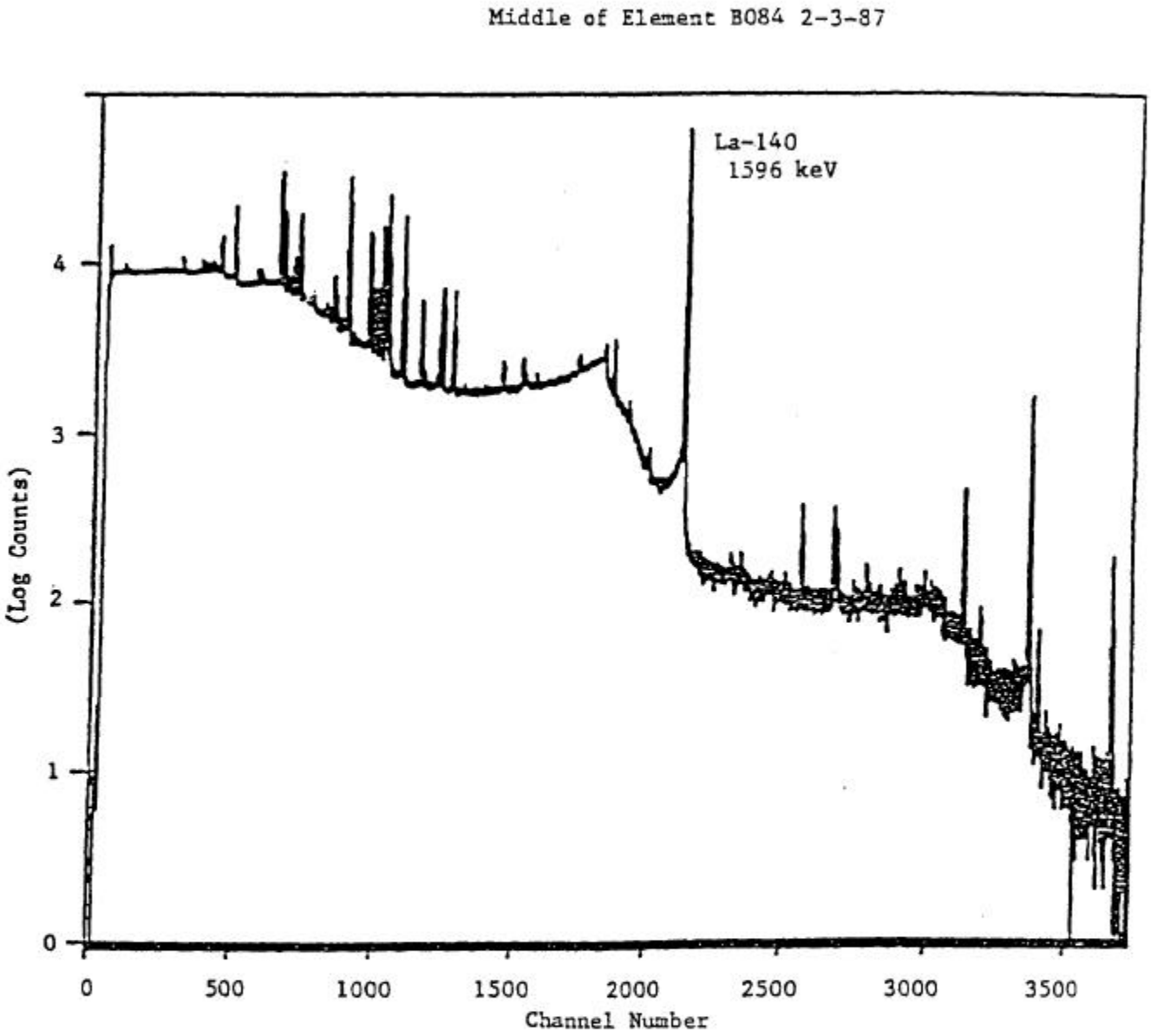

Fig. 8. Gamma Spectrum of LEU Fuel

5. COMPUTER CODES AND MODELS

5.1 Multigroup Cross Sections (EPRI-CELL Code)

The EPRI-CELL code,[14] modified at ANL to include slab geometry, was used to generate broad-group, burnup-dependent cross sections and homogenized atom densities for subsequent diffusion theory calculations. EPRI-CELL combines the GAM[15] resonance treatment in the epithermal energy range with a THERMOS[16] heterogeneous, integral transport treatment in the thermal energy range. As input, the code utilizes a 68-group fast GAM library and a 35-group slow THERMOS library. These libraries have been updated with ENDF/B-IV data processed either through the XLACS2 module of the AMPX system[l7] or by the NJOY code[18] for the thermal library and by the MC^2-2 code[19] for the fast library.

For a specified cell geometry (cylinder or slab) EPRI-CELL performs a one-dimensional transport calculation to determine the neutron spectrum as a function of space, energy, and burnup. Broad-group cross sections result from collapsing the GAM/THERMOS cross sections over this spectrum. Considerable flexibility is available for choosing the number and energy boundaries of the broad groups. However, the boundary between the fast and thermal groups is fixed at 1.855 eV. Tables 9 and 10 show the energy structure of the fast GAM and slow THERMOS libraries while Table 11 gives the standard 5-broad-group structure used in these studies.

EPRI-CELL was used to generate 5-group cross sections for each region in the reactor. For this purpose each fuel element was represented by a fuel region and a side plate region. Burnup-dependent cross sections for the fuel region were obtained from a meat-clad-moderator unit cell calculation. For the side plate region (H_20/Al) cross sections were obtained by collapsing the fine-group cross sections over the neutron spectrum in the XTRA region of a meat-clad-moderator-XTRA unit cell. The composition of the XTRA region was chosen so as to preserve the volume fractions of materials in the fuel element beyond the width of the fuel meat.

5.2 Diffusion Calculations (DIF3D Code)

Most of the calculations in this study were done within the framework of diffusion theory. The DIF3D code[20] was used for this purpose. DIF3D uses the mesh-centered finite-difference approximation to obtain numerical solutions to the multigroup diffusion equations in one-, two-, and three-dimensional geometries.

5.3 Burnup Calculations (REBUS-3 Code)

REBUS-3[21] is a system of codes designed for the analysis of reactor fuel cycles. It solves two basic types of problems:

1 . the infinite time, or equilibrium, conditions of a reactor operating under a fixed fuel management scheme, and

2. the explicit cycle-by-cycle, or non-equilibrium, operation of a reactor under a specified repetitive or non-repetitive fuel management program.

Finite difference, spatial flux synthesis, or nodal diffusion- theory methods are optionally available in the REBUS-3 code system to provide the flux solution in one, two, or three dimensions.

Table 9. Group Structure of the Fast GAM Library

Group Number	Upper Energy of Group (eV)	Group Number	Upper Energy of Group (eV)	Group Number	Upper Energy of Group (eV)
1	1.0000E+7	24	3.1824E+4	47	1.0130E+2
2	7.7880E+6	25	2.4788E+4	48	7.8893E+2
3	6.0653E+6	26	1.9309E+4	49	6.1442E+2
4	4.7237E+6	27	1.5034E+4	50	4.7851E+1
5	3.6788E+6	28	1.1709E+4	51	3.7267E+1
6	2.8650E+6	29	9.1188E+3	52	2.9023E+1
7	2.2313E+6	30	7.1018E+3	53	2.2603E+1
8	1.7377E+6	31	5.5309E+3	54	1. 7604E+1
9	1.3534E+6	32	4.3074E+3	55	1.3710E+1
10	1.0540E+6	33	3.3546E+3	56	1.0677E+1
11	8.2085E+5	34	2.6126E+3	57	8.3153
12	6.3928E+5	35	2.0347E+3	58	6.4760
13	4.9787E+5	36	1.5846E+3	59	5.0435
14	3.8774E+5	37	1.2341E+3	60	3.9279
15	3.0197E+5	38	9.6112E +2	61	3.0590
16	2.3518E+5	39	7.4852E +2	62	2.3824
17	1.8316E+5	40	5.8295E +2	63	1.8550
18	1.4264E+5	41	4.5400E+2	64	1.4450
19	1. 1109E+5	42	3.5358E+2	65	1.1254
20	8.6517E+4	43	2.7536E+2	66	8.7643E-1
21	6.7380E+4	44	2.1445E+2	67	6.8256E-1
22	5.2475E+4	45	1.6702E+2	68	5.3458E-1
23	4.0868E+4	46	1.8109E+2	69	4.1400E-I

Table 10. Group Structure of the Slow THERMOS Library

Group Number	Lower Energy of Group (eV)	Group Number	Lower Energy of Group (eV)
1	1.0000E-5	19	3.5768E-1
2	2.2770E-3	20	4.1704E-1
3	6.3250E-3	21	5.0326E-1
4	1.2397E-2	22	6.2493E-1
5	2.0493E-2	23	7.8211E-1
6	3.0613E-2	24	9.5070E-1
7	4.2757E-2	25	1.0137
8	5.6925E-2	26	1.0428
9	8.1972E-2	27	1.0525
10	1.1157E-1	28	1.0624
11	1.4573E-1	29	1.0722
12	1.8444E-1	30	1.0987
13	2.2770E-1	31	1.1664
14	2.5104E-1	32	1.3079
15	2.7053E-1	33	1.4575
16	2.9075E-1	34	1.5950
17	3.0113E-1	35	1.7262
18	3.2064E-1	36	1.8550

Table 11. Standard 5-Group Structure

Group Number	Upper Energy of Group (eV)
1	1.000E+7
2	8.2085E+5
3	5.53084E3
4	1.8554
5	6.24933E-

REBUS-3 with the three-dimensional finite-difference diffusion-theory option was used to analyze the burnup behavior of each fuel element in each reactor cycle. All the cores were analyzed by the REBUS-3 code as non-equilibrium problems. The code allows the use of' burnup-dependent cross sections and control rod movement during the bum cycle. In most of these calculations the bum cycle length, determined from the total MWh's of reactor operation, was divided into three equal subintervals. Critical control rod positions at the boundaries of each of these sub intervals were determined from the recorded control rod position history and input into the REBUS depletion problem. At each of these boundaries, or time nodes, the code determines burnup-dependent atom densities in six axial regions of equal height for each fuel element, the eigenvalue, fuel element powers, and neutron fluxes. From numerous REBUS calculations a library of axially dependent atom densities for partially burned fuel elements and fuel follower elements was obtained for use in subsequent calculations. These atom densities are appropriately adjusted for the shutdown decay.

The poison section of each shim rod consists of a square, water-filled cadmium annulus 0.040" thick, 2.34" on a side, and 30.5" long. It was shown in Ref. 22 that these cadmium control elements may be represented in a diffusion calculation by using blackness-modified effective diffusion parameters in which the cadmium is black to group 5-neutrons (E_n<0.625 eV). In the normal operation of the ORR, shim rods F4 and F6 are fully withdrawn while the other four (134, 136, D4, and 136) are banked together at a position to achieve criticality.

5.4 Monte Carlo Calculations (VIM Code)

The VIM code[23] is a continuous energy, three-dimensional, Monte Carlo code used mostly for criticality calculations. VIM calculates eigenvalues by analog collision and track length estimation. Both collision and track length estimation are used to provide reaction rate estimates by region, group and/or isotope. Group and region-integrated fluxes are provided by track length estimation. Broad-group, region-dependent, microscopic cross sections are obtained from the track length estimation of reaction rates and fluxes. However, VIM does not calculate scattering arrays.

The VIM code was used in this study to determine eigenvalues and reaction rate distributions in the water- and beryllium-reflected criticals with unirradiated HEU and LEU fuel. These results have been compared with DIF313 calculations and will be discussed in Section 7. 1.

VIM was also used to investigate the effect of ENDF/B-IV versus ENDF/B-V cross sections on ORR calculations. Three important changes were made in the ENDF/B-V data files which may influence thermal reactor calculations:

1. The ^{235}U prompt neutron fission spectrum has been hardened. ENDF/B-V uses a prompt Watt spectrum with E = 2.030 MeV whereas ENDF/B-IV used a Maxwellian spectrum with E = 1.985 MeV.

2. ENDF/B-V incorporates new and improved ^{238}U resonance parameters. This results in reduced ^{238}U capture relative to ENDF[B-IV.

3. The thermal value of V for ^{235}U has been increased by 0.74% relative to that used in ENDF/B-IV.

In order to evaluate the effects of these changes, the ORR beryllium-reflected fresh LEU critical core (179AX6) was chosen for a test case. Identical VIM Monte Carlo calculations were performed for this core using cross sections (300K) based on ENDF/B-IV and again on ENDF/B-V. The calculated eigenvalues for the experimentally determined critical system are shown below. They are based on 300,000 neutron histories.

	ENDB/B-IV	ENDB/B-V
Eigenvalue:	1.0033 ± 0.0019	1.0030 ± 0.0018

Region-averaged multigroup cross sections are compared in Table 12 and region-averaged neutron spectra are compared in Table 13. The statistical errors are obtained from the VIM calculations and correspond to one standard deviation. These tables illustrate the ENDF/B-V changes discussed above.

In the intermediate energy range (groups 2 and 3) the ^{238}U fission cross section has been significantly increased in ENDF/B-V. However, only 0.5% of the fission events in the ORR LEU critical occur in ^{238}U and 99.8% of these are in group I where the ENDF/B-IV and ENDF/B-V ^{238}U fission cross sections are the same.

These results show that, at least for the beryllium-reflected ORR critical, analyses based on the use of ENDF/B-IV cross sections are fully justified. Changes resulting from the use of the ENDF/B-V data base are negligible.

5.5 Transport Calculations (TWODANT Code)

The TWODANT code[24] solves the two-dimensional multigroup transport equation in xy, rz, and rϑ geometries. Both regular and adjoint, homogeneous (eigenvalue) and inhomogeneous (fixed source) problems are solved subject to vacuum, reflective, periodic, or white boundary conditions. TWODANT solves the two-dimensional, multigroup, steady-state Boltzmann transport equation in the discrete-ordinates approximation. Inner and outer iterations are accelerated using the diffusion synthetic acceleration method.

There are six evacuated beam tubes (6-7/8" ID) which leave the east side of the aluminum core box at various angles. Two-dimensional xy transport calculations were performed to study the influence of these evacuated beam tubes on flux and power distributions in the core. By comparing these results with corresponding xy diffusion calculations it was found that the perturbing effect of the beam tubes could be represented approximately in DIF3D calculations by filling the beam tubes with water at about 3% of normal density. However, these xy studies suffer from the fact that they do not allow one to model the actual three-dimensional character of the beam tubes nor do they permit one to model the real angles at which the beam tubes exit the aluminum core box. For these reasons beam tube effects were studied using the Monte Carlo code, VIM. Calculations were done for the case of voided beam tubes and for the case of beam tubes flooded with water at normal density for core 177-AX1. Similar xyz calculations were made with the DIF3D diffusion code where the "voided" case corresponded to water at 3% of normal density. The following observations were made on the basis of these calculations:

1. The two types of calculations are consistent in their predictions of the amount by which the eigenvalue is lowered due to neutron leakage through the voided beam tubes relative to the flooded case.

Calculation	Delta k-eff., %
VIM-Monte Carlo	-0.73 ± 0.33
DIF3D-Diffusion	-0.493

Table 12. ENDF/B-V to ENDF/B-IV Region-Averaged Cross Section Ratios
ENDF/B-V to ENDF/B-IV Ratio

Region	Element Isotope	Cross Section	Group 1	Group 2	Group 3	Group 4	Group 5
H,O-Refl.	^{1}H	(n,γ)	1.0012 ± 0.0026	1.0026 ± 0.0081	0.9974 ± 0.0057	0.9995 ± 0.0018	1.0015 ± 0.0008
H,O-Refl.	^{1}H	(n,γ)	1.0007 ± 0.0056	0.9948 ± 0.0038	1.0003 ± 0.0001	0.9999 ± 0.0002	1.0016 ± 0.0007
Be-Refl.	^{9}Be	(n,γ)	0.9961 ± 0.0044	1.0045 ± 0.0014	0.9993 ± 0.0019	1.0010 ± 0.0007	1.0020 ± 0.0013
Be-Refl.	^{9}Be	(n,γ)	0.9994 ± 0.0014	0.9992 ± 0.0004	1.0000 ± 0.0000	0.9939 ± 0.0030	0.9997 ± 0.0006
Core	^{235}U	(n,γ)	0.9890 + 0.0020	0.9958 ± 0.0018	1.0092 ± 0.0045	1.0016 ± 0.0059	1.0079 ± 0.0025
Core	^{235}U	(n,γ)	0.9890 ± 0.0020	0.9958 ± 0.0018	1.0092 ± 0.0045	1.0016 ± 0.0050	1.0079 ± 0.0025
Core	^{235}U	(n,γ)	0.9899 ± 0.0031	0.9968 ± 0.0027	1.0021 ± 0.0065	1.0404 ± 0.0075	0.9998 ± 0.0024
Core	^{238}U	(n,γ)	0.9925 ± 0.0034	1.0045 ± 0.0031	0.9839 ± 0.0155	0.9795 ± 0.0042	1.0029 ± 0.0020
Core	^{27}Al	(n,γ)	0.9516 + 0.0134	0.9994 ± 0.0100	1.0064 ± 0.0032	0.9967 ± 0.0041	0.9996 ± 0.0037
Core	Si	(n,γ)	0.9539 ± 0.0208	1.7524 ± 0.0144	1.0917 ± 0.0041	1.0005 ± 0.0043	1.0029 ± 0.0024
Control Rod	Cd	(n,γ)	0.9943 ± 0.0138	0.9938 ± 0.0253	0.9197 ± 0.0536	1.0150 ± 0.0381	1.0114 ± 0.0300

Table 13. ENDF/B-V-to-ENDF/B-TV Region-Integrated Spectrum Ratios
ENDF/B-V to ENDF/B-IV Ratio

Region	Group 1	Group 2	Group 3	Group 4	Group 5
H_20-Refl.	0.9868 ± 0.0227	1.0063 ± 0.0152	0.9970 ± 0.0115	1.0123 ± 0.0155	1.0047 ± 0.0108
Be-Refl.	1.0193 ± 0.0066	1.0050 ± 0.0053	0.9962 ± 0.0053	0.9919 ± 0.0073	0.9972 ± 0.0076
Core	1.0298 ± 0.0045	0.9845 ± 0.0042	0.9934 ± 0.0041	0.9847 ± 0.0069	0.9935 ± 0.0052

2. Within the statistics of the Monte Carlo calculations (based on 200,000 neutron histories), the voided-to-flooded ratio of the region-integrated fission rates for VIM and DIF3D agree

	Voided-to-Flooded Fission Rate Ratio	
Row	VIM-Monte Carlo	DIF3D
A	1.032 ± 0.015	1.025
B	1.039 ± 0.017	1.021
C	1.021 ± 0.013	1.011
D	0.983 ± 0.011	1.001
E	0.978 ± 0.014	0.982
F	0.942 ± 0.011	0.950

The statistical errors correspond to one standard deviation. Beam tubes exit from the outer edge of row F.

Based on these observations it is concluded that the 3% water density model is an adequate representation of the ORR voided beam tubes in DIF3D calculations.

5.6 Calculation of Kinetic Parameters (VAR13D Code)

The VAR13D code[25] is a three-dimensional perturbation theory code. Beginning with flux distributions and burnup-dependent cross sections and atom densities for REBUS-3 calculations, the VAR13D code was used to determine the adjoint flux and the effective delayed neutron fraction. In addition, the code evaluates a 6-family coalesced set of the kinetic parameters (λ_i,β_i) from ENDF/B-V delayed neutron data.

5.7 ^{6}Li and ^{3}He Poisons in Beryllium

Because of neutron-induced reactions, ^{6}Li and ^{3}He poisons build up in the beryllium and need to be taken into account in the calculations. The process begins with the fast neutron threshold reaction

^{9}Be(n α)^{6}He $\qquad E_n > 0.67$ MeV

and the poisons result from the subsequent reactions

'He $\beta^- \rightarrow {}^6$Li $\qquad T_{1/2} = 0.80$ sec

^{6}Li(n,α)^{3}H $\qquad \sigma_\alpha$(th) = 940 ± 4 b

^{3}H $\beta^- \rightarrow {}^3$He $\qquad T_{1/2} = 12.35$ yr

^{3}He(n,p)^{3}H $\qquad \sigma_P$(th) = 5333 ± 7 b

The equations for the time-dependent atom concentrations are

$$dN_1/dt = N(Be) \sum_{i=1}^{5} \sigma_{\alpha i}(Be)\, \phi_i - N_1 \sum_{i=1}^{5} [\sigma_{\alpha i}(^6Li) + \sigma_{\gamma i}(^6Li)]\, \phi_i$$

$$dN_2/dt = N_1 \sum_{i=1}^{5} \sigma_{\alpha i}(^6Li)\, \phi_i - \lambda_2 N_2 + N_3 \sum_{i=1}^{5} \sigma_{pi}(^3He)\, \phi_i - N_2 \sum_{i=1}^{5} \sigma_{\gamma i}(^3H)\, \phi_i$$

$$dN_3/dt = \lambda_2 N_2 - N_3 \sum_{i=1}^{5} [\sigma_{pi}(^3He) + \sigma_{\gamma i}(^3He)]\, \phi_i$$

where the subscripts 1, 2, and 3 refer to ^{6}Li, ^{3}H, and ^{3}He, respectively, where λ_2 is the tritium decay constant, and where the decay of ^{6}He is assumed to be instantaneous. Since the (n, γ) capture rates are totally negligible relative to the (n, α) and (n,p) processes, these equations reduce to

$$dN_1/dt = A - B\, N_1$$

$$dN_2/dt = B\, N_1 - \lambda_2 N_2 + C\, N_3$$

$$dN_3/dt = \lambda_2 N_2 - C\, N_3$$

where the constants are defined as

$$A \equiv N(Be) \sum_{i=1}^{5} \sigma_{\alpha i}(Be)\, \phi_i$$

$$B \equiv \sum_{i=1}^{5} \sigma_{\alpha i}(^6Li)\, \phi_i$$

$$C \equiv \sum_{i=1}^{5} \sigma_{pi}(^3He)\, \phi_i\,.$$

Standard methods are used to solve this set of simultaneous differential equations. The general solutions for the atom densities are

$$N_{Li6}(t) = N_1(0)e^{-Bt} + \frac{A}{B}(1 - e^{-Bt})$$

$$N_{H3}(t) = a_1 + a_2 e^{-(\lambda_2+C)t} + \frac{AC}{\lambda_2+C}t + \frac{(C-B)[N_1(0) - A/B]\, e^{-Bt}}{B-(\lambda_2+C)}$$

$$N_{He3}(t) = \frac{\lambda_2}{C}a_1 - a_2 e^{-(\lambda_2+C)t} + \frac{\lambda_2 A}{\lambda_2+C}(t-1/C) + \frac{\lambda_2[N_1(0)-A/B]e^{-Bt}}{B-(\lambda_2+C)}$$

where the integration constants, a_1 and a_2, follow from the initial conditions,

$$a_1 \equiv [N_1(0) + N_2(0) + N_3(0) - \frac{A}{B} + \frac{\lambda_2 A/C}{\lambda_2+C}]/(1 + \lambda_2/C)$$

$$a_2 \equiv [\frac{B}{(B-\lambda_2-C)}(N_1(0) - A/B) + N_2(0) - \frac{C}{\lambda_2}N_3(0) - \frac{A}{\lambda_2+C}]/(1 + C/\lambda_2)$$

The first of these solutions shows that the ^{6}Li concentration reaches 99% of its saturated value (A/B) in an irradiation time of 4.605/B. Since $(\lambda_2 + C)>B$, it follows that by the time the ^{6}Li concentration saturates the ^{3}H and ^{3}He atom densities increase linearly in time with slopes of $AC/(\lambda_2 + C)$ and $\lambda_2 A/(\lambda_2 + C)$, respectively.

These results have been applied to the 30-MW Oak Ridge Research Reactor. For neutron fluxes averaged over the beryllium reflector region the constants take on the values

$$A = 1.32510 \times 10^{-13} \text{ (b - cm sec)}^{-1}$$
$$B = 1.27315 \times 10^{-7} \text{ sec}^{-1}$$
$$C = 7.21223 \times 10^{-7} \text{ sec}^{-1}$$

Figure 9 shows how the ^{6}Li, ^{3}H, and ^{3}He concentrations build up in the beryllium reflector for the reactor operating at 30 MW, assuming the atom densities of the poisons are initially zero. The saturated ^{6}Li concentration is A/B = 1.40804 x 10-6 atoms/b - cm, and the time to reach 99% of this value is 4.605/B = 1.146 ear. By this time the ^{3}H and ^{3}He densities increase linearly in time with slopes of 1. 1327 x 10^{-8} and 2.81629 x 10^{-11} atoms/b-cm-day, respectively.

Figure 10 shows how the ^{3}He concentration in the beryllium reflector changes with time for two different sets of initial atom densities. In both cases the beryllium reflector was assumed to have been irradiated continuously over a 10-year period with the reactor operating at 30 MW. In one case, following the 10-year irradiation, the beryllium reflector elements were placed in storage for a 2-year period during which time the ^{3}He content increased due to the β-decay of tritium. No storage period was allowed in the second case. It follows that 99% of the excess He bums out of the reflector in an exposure time of $4.605/(\lambda_2 + C) = 0.202$ yr (see Fig. 10). Because the tritium concentration is several orders of magnitude larger than the ^{3}He density, even short decay periods can result in a significant increase in the poisoning effect of ^{3}He.

The reactivity associated with the ^{6}Li and ^{3}He poisons in the ORR beryllium reflector were estimated using one-group perturbation theory. Results from these reactivity buildup calculations are shown in Figs. 11 and 12. Use of one-group perturbation theory tends to overestimate the 6Li and 3He reactivities by about 10-20%. Typical cycle lengths in the ORR are 2-3 weeks. For these times the initial concentrations of the poisons in the beryllium are far more important than the small changes which occur during the operating cycle. It is usually necessary to account for the buildup of ^{3}He due to the decay of ^{3}H during the shutdown period between cycles.

The buildup and burnout of ^{6}Li and ^{3}He in all the beryllium regions in the ORR has been taken into account in the REBUS-3 burnup calculations. These calculations include the production of ^{3}He from the decay of tritium during the shutdown periods.

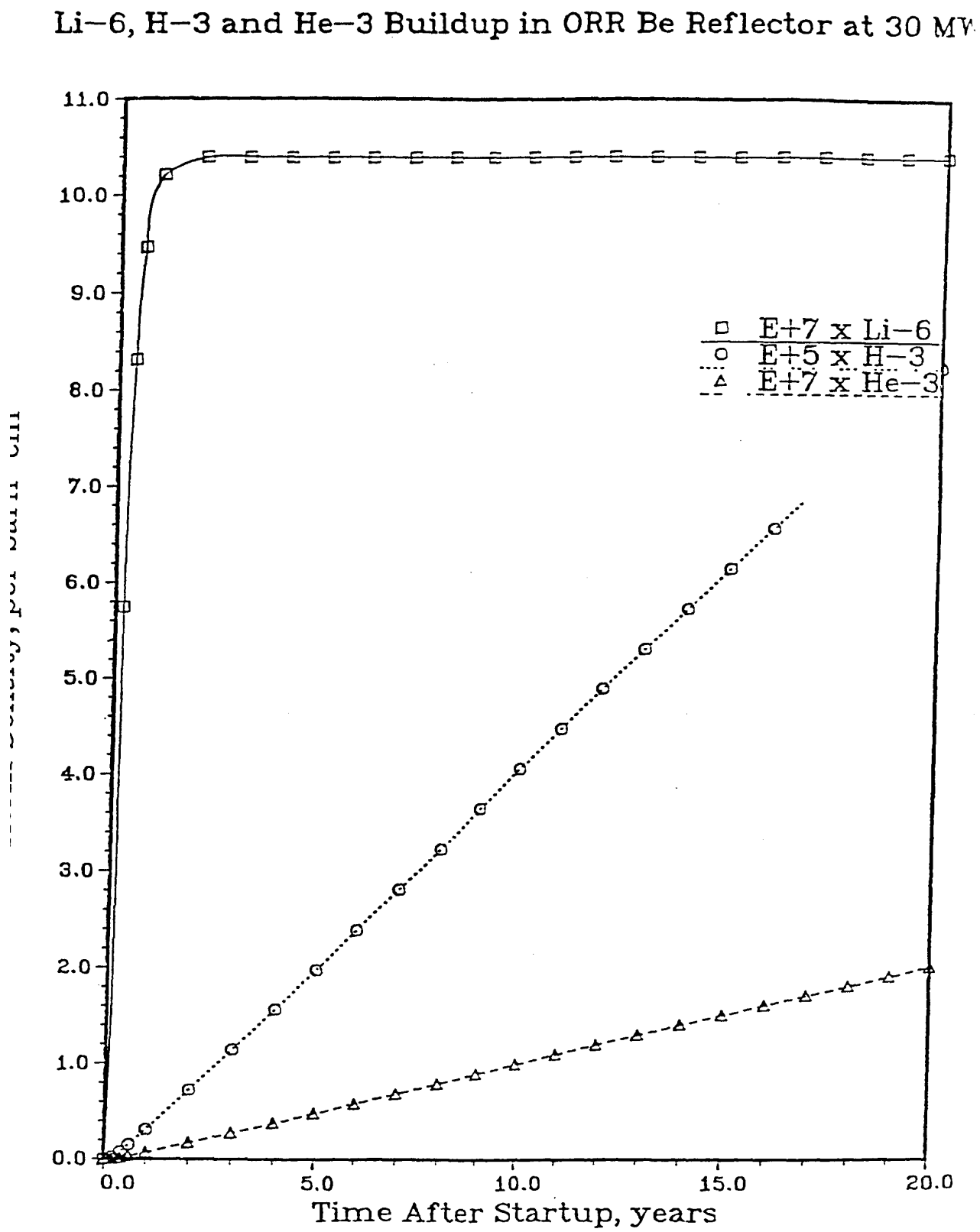
Li–6, H–3 and He–3 Buildup in ORR Be Reflector at 30 MW
11.0
10.0
9.0
8.0
7.0
6.0
5.0
4.0
3.0
2.0
1.0
0.0
0.0
5.0
10.0
15.0
20.0
Time After Startup, years
E+7 x Li–6
E+5 x H–3
E+7 x He–3

Fig. 9

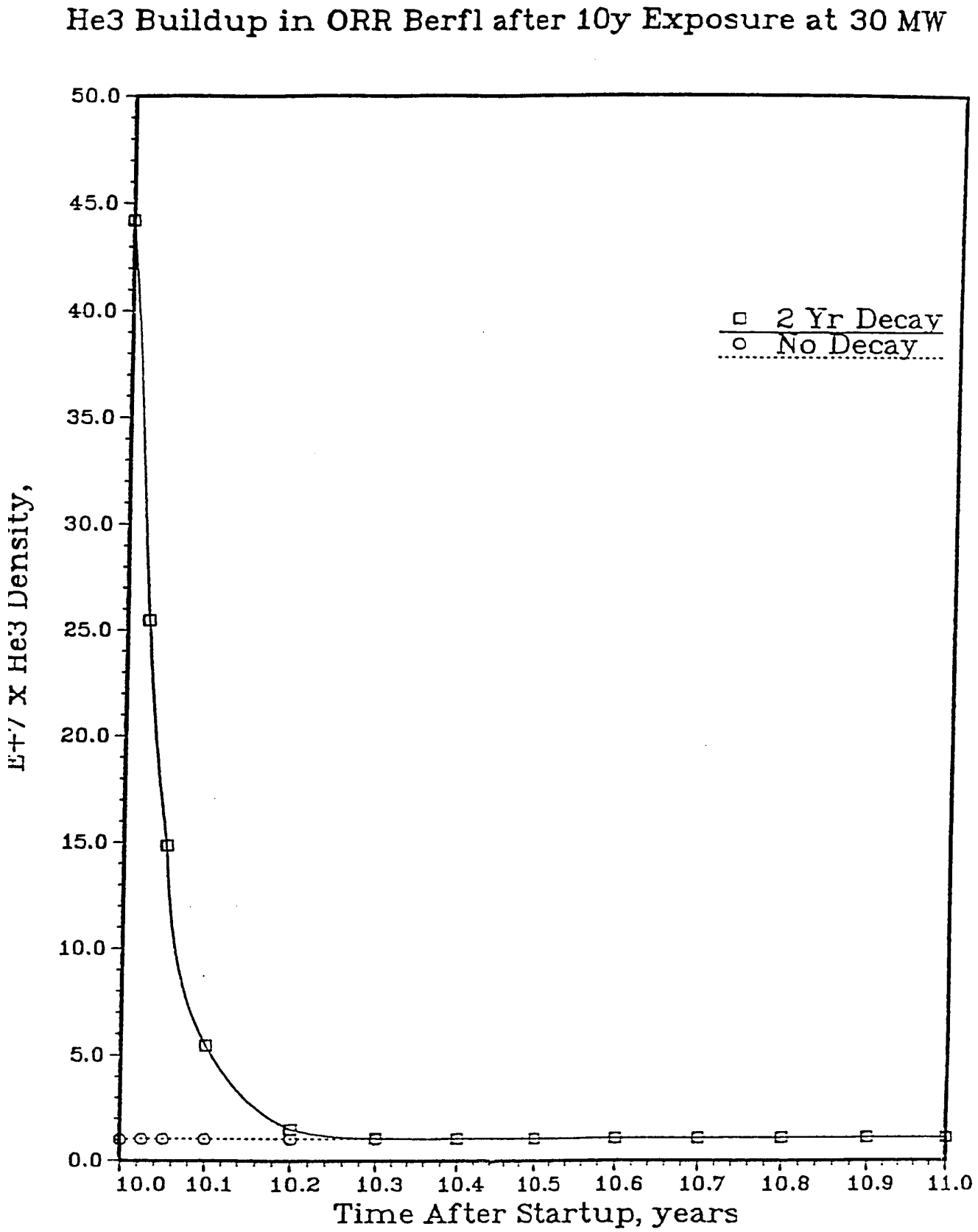
He3 Buildup in ORR Berfl after 10y Exposure at 30 MW
50.0
45.0
40.0
35.0
30.0
25.0
20.0
15.0
10.0
5.0
0.0
E+7 x He3 Density,
2 Yr Decay
No Decay
10.0
10.1
10.2
10.3
10.4
10.5
10.6
10.7
10.8
10.9
11.0
Time After Startup, years

Fig. 10

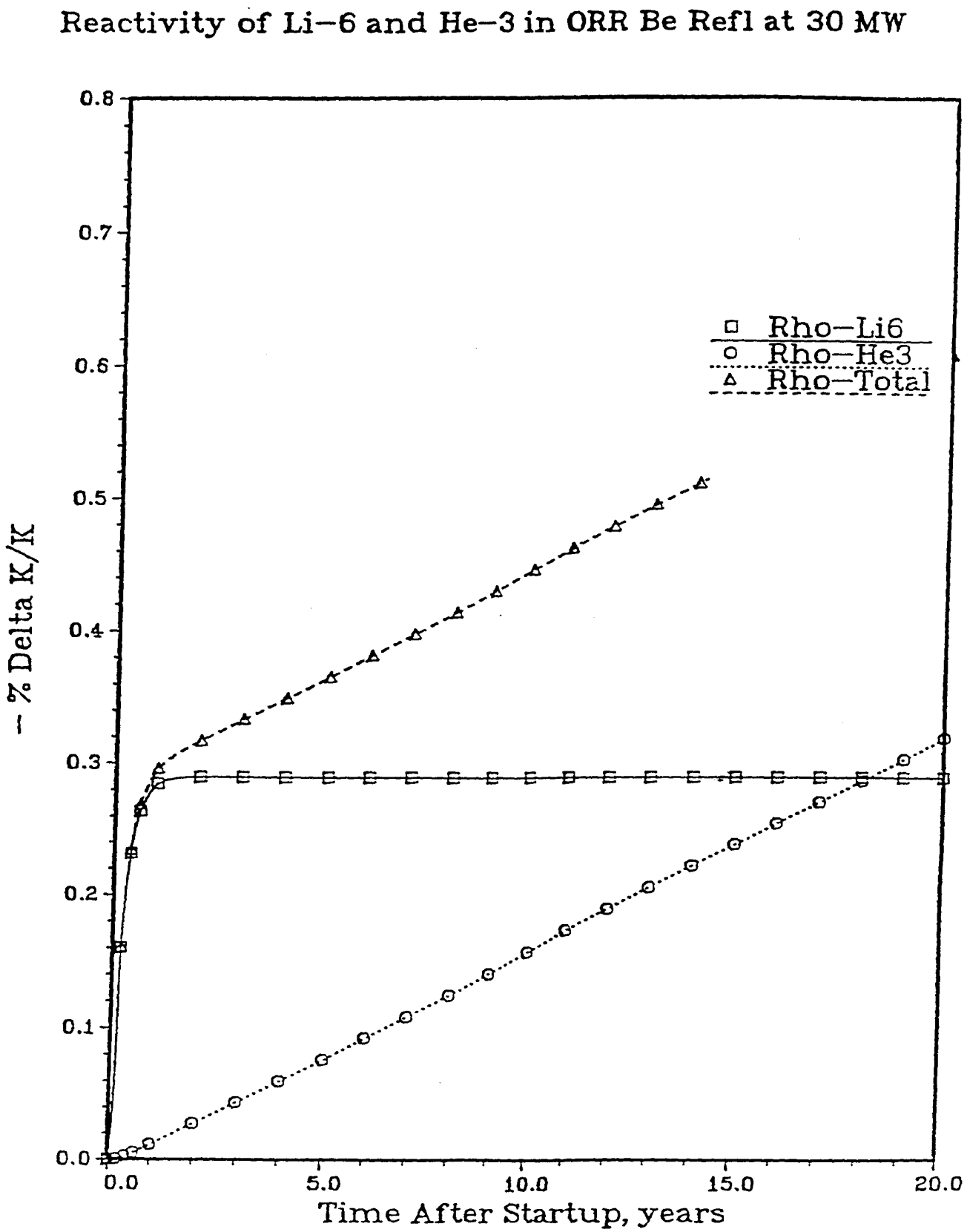
Reactivity of Li-6 and He-3 in ORR Be Refl at 30 MW
Rho-Li6
Rho-He3
Rho-Total
- % Delta K/K
0.0
0.1
0.2
0.3
0.4
0.5
0.6
0.7
0.8
0.0
5.0
10.0
15.0
20.0
Time After Startup, years

Fig. 11

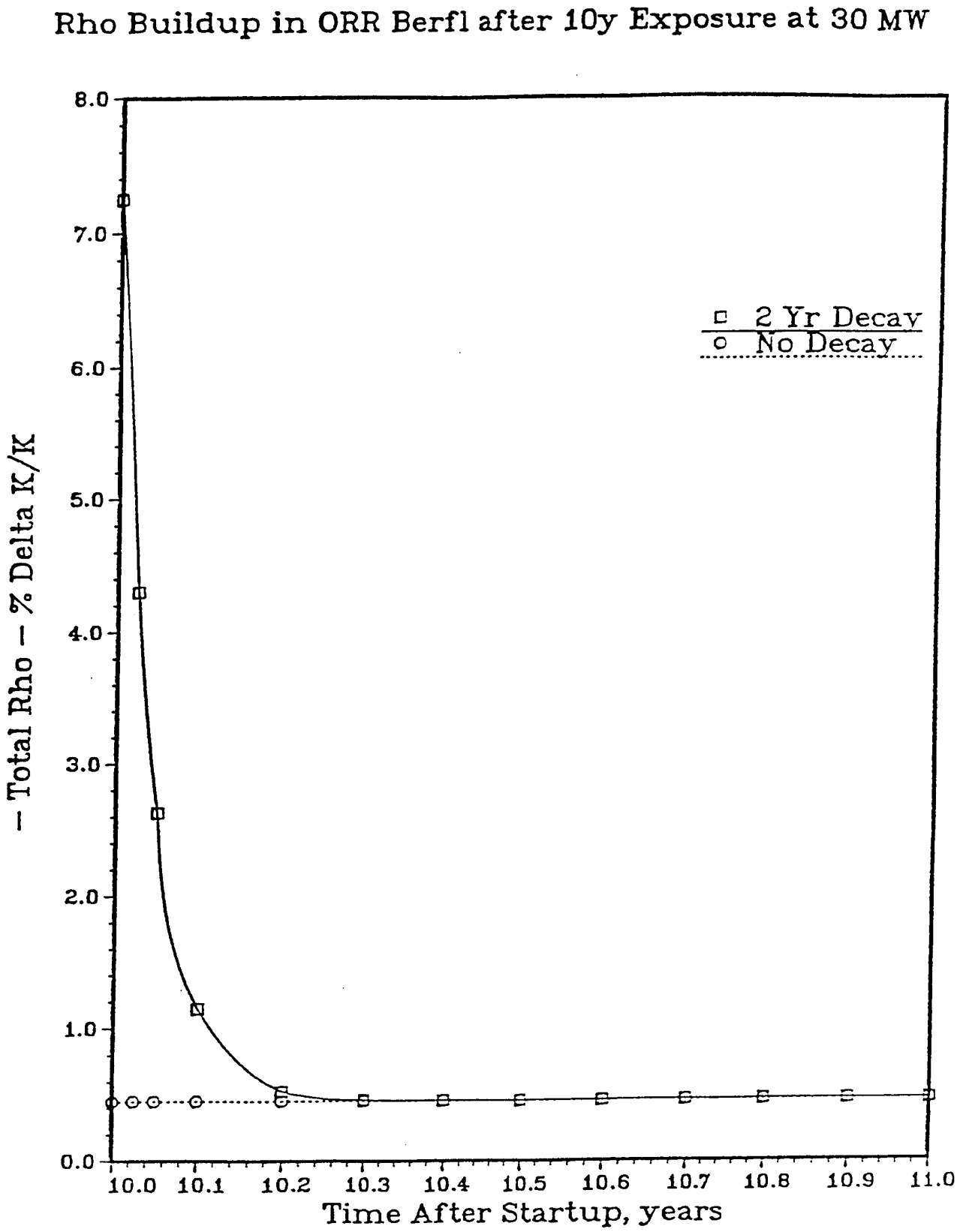
Rho Buildup in ORR Berfl after 10y Exposure at 30 MW
8.0
7.0
6.0
5.0
4.0
3.0
2.0
1.0
0.0
– Total Rho – % Delta K/K
2 Yr Decay
No Decay
10.0
10.1
10.2
10.3
10.4
10.5
10.6
10.7
10.8
10.9
11.0
Time After Startup, years

Fig. 12

5.8 3D Model of the ORR

The axial elevations of the ORR control rods are assymetric with respect to the core midplane and vary throughout the bum cycle in order to maintain criticality. For this reason and because the compositions of the MFE's are axially assymetric, it was necessary to model the ORR in three dimensions in order to perform burnup calculations based on diffusion theory. The overall x, y, and z dimensions of the 3D model were 130.825 cm x 141.385 cm x 217.217 cm, with the y-direction chosen to be perpendicular to the fuel plates. Because of different core configurations (see Appendix A), the mesh structure varied somewhat from core to core. Typically, the number of mesh intervals in the x, y, and z directions was 65 x 65 x 53, respectively. Some of the features of this 3D model are described below. The 3D model used to analyze one of the water-reflected fresh criticals is described in detail in Appendix D.

5.8.1 Fuel Elements

Each fuel element is individually represented in the calculations. The element is divided into six homogenized (meat, cladding, moderator) axial fuel zones of equal height (10.00 cm), into side plate regions, and into axial reflector regions. Extending beyond the width of the fuel meat, the side plate regions allow for flux peaking in the homogenized mixture of aluminum and water. The homogenized axial reflector regions allow for the fuel plate extensions beyond the height of the fuel column as well as for the aluminum end boxes. Axially dependent atom densities are stored for each time node in the REBUS-3 fuel depletion calculations for subsequent use. Five mesh intervals each of 1 cm width are provided above and below the fuel column to allow for an adequate calculation of flux peaking in the axial reflectors.

5.8.2 Shim Rod Assemblies

The lower fuel follower sections of the shim rods are modeled in a manner similar to the standard fuel elements including explicit side plate regions and six homogenized axial fuel zones. A 2-inch transition region exists between the top of the fuel column and the bottom of the poison section. The poison consists of a square, hollow cadmium box 2.3 inches on a side, 30.5 inches long, and 0.040 inch thick and is modeled explicitly. Homogenized aluminum-water compositions with appropriate volume fractions are used to represent the transition region and the regions inside and outside the cadmium box. With the shim rods fully inserted the cadmium poison is symmetrically positioned about the axial midplane of the core. In the model the z=0 plane corresponds to the bottom of a fully inserted shim rod. Thermal neutron absorption in the cadmium is treated in terms of an appropriate set of internal boundary conditions (i.e. current-to-flux ratios) applied at the surface of the cadmium.

5.8.3 Beryllium Reflector

The beryllium reflector elements are 31.38 inches long. To account for the small amount of water outside the reflector element and that in the 3/16-inch central coolant hole, the reflector composition was chosen as a homogenized composition of beryllium and water. As discussed in Section 5.7, the ^{6}Li and ^{3}He poisons in the beryllium are included in the calculations. Small impurities in the beryllium have been treated in terms of an equivalent ^{10}B concentration of equal neutron absorption.

5.8.4 Experimental Facilities

The six voided beam tubes on the east side of the core are explicitly represented in the DIF3D model. Effects of neutron leakage through the beam tubes are approximately included by choosing a beam tube composition corresponding to water at about 3% of normal density.

The gamma shield and pressure vessel simulator, which constitute the HSST experiment on the west side of the core, are explicitly modeled. Homogenized compositions for these facilities have been supplied by ORNL personnel. For those cores operated with the HSST withdrawn, the compositions of the gamma ray shield and pressure vessel simulator were replaced with water.

Engineering facilities are located on the north and south sides of the core. However, detailed information regarding the structure and composition of these facilities was not available. Therefore, they were replaced with pool water and not represented in the model.

Radioactive isotopes of europiurn and iridium were produced in hollow beryllium elements located in reflector (Eu) and core (Ir) positions. Europium and iridium samples were mounted on the surface of the central portion of cylindrical aluminum stringers which fit into the hollow beryllium elements. The hollow portion of the beryllium element was divided into three axial zones with the irradiation sample located in the central zone. The composition of the two outer axial zones was an homogenized mixture of aluminum and water while the composition of the central zone included the europium (or iridium) sample. Since the EPRI-CELL library does not include iridium because this element is not part of the ENDF/B file, this material was described by a mixture of gold and ^{6}Li with the relative concentrations chosen so as to reproduce the iridium resonance integral and thermal neutron absorption cross section. Again, ^{6}Li and ^{3}He poisons were included in the beryllium portion of the isotope irradiation facilities.

The magnetic fusion experiments, MFE-7J and MFE-6J, were located in grid positions C3 and C7, respectively. Axially-dependent material volume fractions for each of these facilities were supplied by ORNL personnel.[4] These volume fractions were used to describe five axial zones needed to model MFE-7J. Similarly, four zones were needed to model MFE-6J.

Miniplate irradiations were conducted in the HFED facility located in grid position E3. The HFED consists of five irradiation modules stacked to a height equal to that of the fuel in the core. Each module was represented explicitly in the DIF3D model with homogenized compositions determined from the loading of the miniature fuel plates.

Numerous reactivity substitution measurements were made, relative to H_20 and/or Al, for the Eu and Ir irradiation modules, and for the MFE, HFEQ, and HSST experiments. In addition, the worths of beryllium reflector elements poisoned with ^{3}He and ^{6}Li were measured relative to unirradiated beryllium. Some of the results of these measurements are summarized in Tables 14 and 15. Since the cross sections used in these evaluations were generated at temperatures somewhat different from the measurements, the calculated eigenvalues had to be temperature adjusted. A calculated temperature coefficient (-1.10 x 10-4/°F) was used for this purpose. The reactivity substitution measurements show that all the experimental facilities are reasonably well modeled in the diffusion calculations.

5.8.5 Core Box and Dummy Fuel Elements

The 6061 aluminum core box which surrounds the beryllium reflector elements and the fuel elements on the west side of the core is included in the model. Neutron absorbing effects in the impurities and in minor elements in the 6061 aluminum alloy were represented by an equal absorption in ^{10}B. The core box model includes:

1. the addition of a thin water gap between the lattice periphery and the inner wall of the box,

2. an effective thickness of the east and west walls of the box to account for the scalloped geometry of the inner surface of these walls, and

Table 14. Reactivity Substitution Measurements for Experimental Facilities Relative to Water

Core	Grid	Sample	Temperature, °F Exp.	Temperature, °F Calc's.	Observed Shim Rod Positions (In.) at Critical F4,F6	B4,B6,D4	D6	k_{eff}
174C	C3	MFE-7J	101.1	140	UL*	14.78	14.78	1.0004
	C3	H_20	100.8	140	UL*	14.55	14.55	1.0024
174C	C7	MFE-6J	101.1	140	UL*	14.78	14.78	1.0004
	C7	H_20	100.8	140	UL*	14.25	14.25	1.0029
174C	E3	HFED	99.7	140	UL*	14.78	14.78	1.0001
	E3	H_20	99.7	140	UL*	14.81	14.81	1.0006
174C	E5	Be + Ir	100.8	140	UL*	14.78	14.78	1.0012
	E5	H_20	100.1	140	UL*	14.98	14.98	1.0022
174C	E7	Be + Ir	100.8	140	UL*	14.78	14.78	1.0012
	E7	H_20	100.0	140	UL*	15.00	15.00	1.0040
174C	B1	Be + Eu	101.1	140	UL*	14.78	14.78	1.0004
	BI	H_20	100.8	140	UL*	14.78	14.48	1.0008
174C	D1	Be + Eu	101.1	140	UL*	14.78	14.78	1.0004
	D1	H_20	100.8	140	UL*	14.78	14.53	1.0014
174C	FI	Be + Eu	101.1	140	UL*	14.78	14.78	1.0004
	Fl	H_20	100.9	140	UL*	14.78	14.58	1.0010
176-AX1		HSST	106.0	140	UL*	14.14	13.60	1.0008
		H_20	106.0	140	UL*	14.14	14.14	0.9998

*UL = upper limit

Table 15. Reactivity Substitution Measurements for Unirradiated Relative to Irradiated Beryllium in Core 174C

New Be Location	Temperature, 'F Exp.	Calcs.	Observed Shim Rod Positions (In.) at Critical F4,F6	B4,B6,D4	D6	K_{eff}
-	100.8	140	UL*	14.78	14.78	1.0043
Al	99.9	140	UL*	14.78	14.70	1.0043
C1	99.9	140	UL*	14.78	14.67	1.0044
El	99.9	140	UL*	14.78	14.65	1.0042
G2	99.9	140	UL*	14.78	14.69	1.0042
F8	99.8	140	UL*	14.78	14.64	1.0042
B8	99.8	140	UL*	14.78	14.61	1.0042

*UL = upper limit

3. an homogenized Al/H_20 composition for the north, west and south walls to account for the coolant holes drilled through these walls.

Near the end of the demonstration dummy fuel elements were located in the comer grid positions (Al, A9, G1, and G9) to improve forced flow conditions. These dummy fuel elements were represented in the model by an appropriate mixture of water and aluminum.

6. DATA ANALYSIS METHODS

This section describes the methods used to analyze the experimental data. Results from these analyses are compared with corresponding analytical calculations in Section [7].

6.1 Cobalt and Gold Wire Activations

In order to minimize the radiation levels from fuel elements used in the fresh criticals, gold wires were activated rather than the cobalt-vanadium wires normally used for this purpose. Since ^{197}Au has a much larger neutron activation cross section than ^{59}Co and because ^{198}Au has a much shorter half-life than ^{60}CO, the gold wires could be activated at substantially lower power levels than those needed for the Co-V wires.

The axial activity distributions were measured at ORNL using a computer-controlled wire scanning system. Data collected by this system were stored on floppy disks and sent to ANL for analysis by R. J. Corriella. Before storage, activities are corrected for background, dead time, and decay since the irradiation. Each wire is identified with regard to the reactor location where it was irradiated. Although the wire locations in the water channels of the standard 19-plate fuel elements are well-known, wire positions in the beryllium elements and in the 15-plate fuel followers are not well-known and are only assumed to be at the center of the assembly.

In order to calculate wire activities, multigroup cross sections were generated by EPRI-CELL.14 One-dimensional cylindrical cell calculations were performed for this purpose in which the wire and its environment were modeled. Broad group gross sections were obtained by collapsing the fine-group wire cross sections over the neutron spectrum in the wire. ^{59}Co and ^{197}Au cross sections were obtained in this manner for both core and beryllium reflector regions.

Axial activity distributions are calculated using these wire cross sections and mesh-centered fluxes obtained from a three-dimensional diffusion theory calculation. A linear interpolation procedure is used to obtain calculated axial activity profiles corresponding to the xy positions where the wires were irradiated.

For wires activated within standard 19-plate fuel elements, the activity profiles are axially offset until the lower and upper reflector valleys are centered with respect to the corresponding analytical profiles. Figure 13 shows an aligned pair of calculated and measured activity profiles including the upper and lower reflector valleys.

A normalization is needed in order to express calculated (C) and measured (E) activity profiles in terms of appropriate C/E ratios. For this purpose, calculated and measured activity profiles are numerically integrated over the height of the fuel. The following equation determines the normalization constant, NORM.

$$\mathrm{NORM} \sum_{i=1}^{n} I_i(C) = \sum_{i=1}^{n} I_i(E)$$

where $I_i(C)$ and $I_i(E)$ are the calculated and measured axially-integrated activities for the ith wire and n is the total number of wires activated in the standard fuel elements.

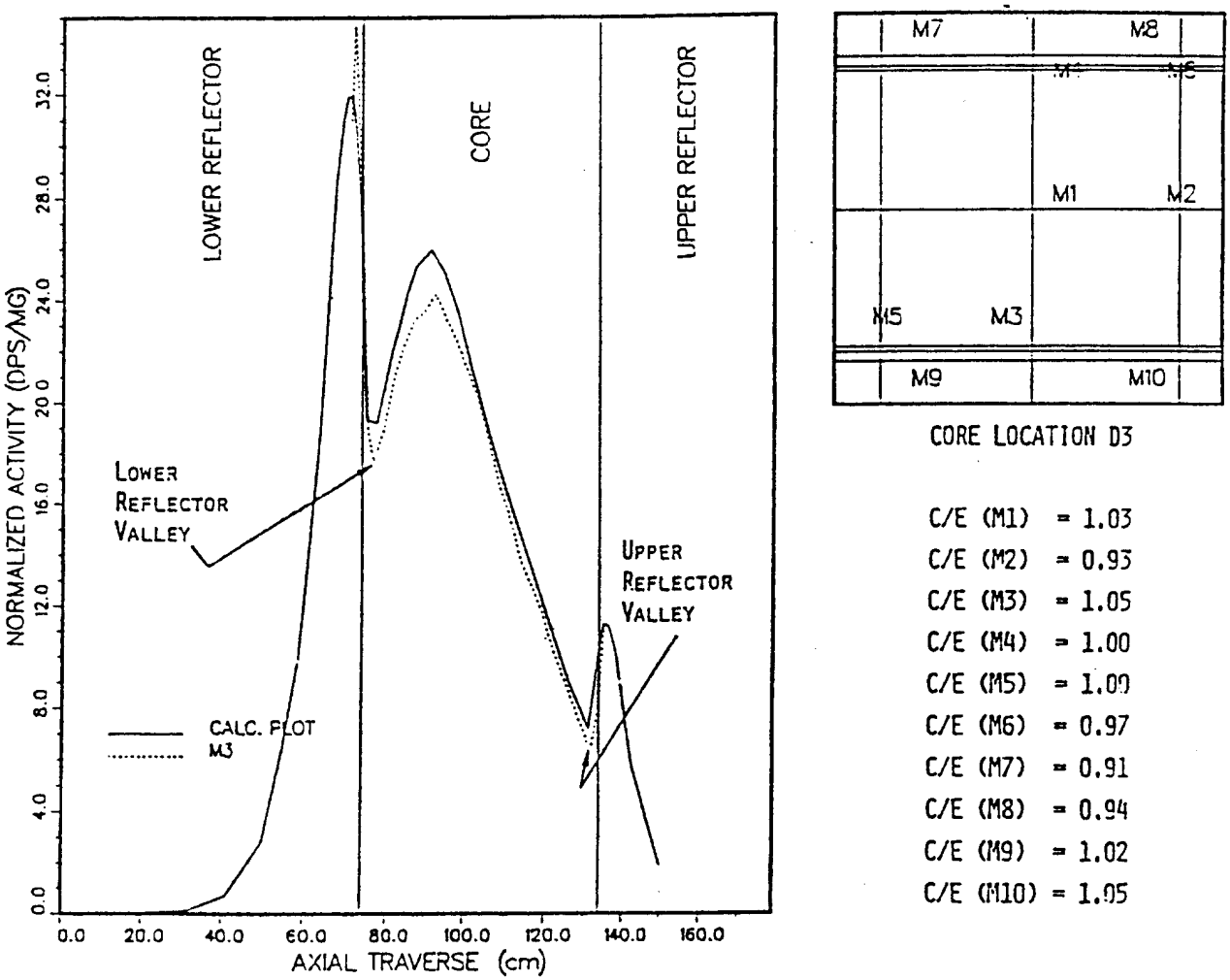

Fig. 13 Calculated and Measured ^{60}Co Activity Profile for Wire M3, Wire Location Superimposed on X-Y Mesh Structure, and the Associated C/E's for Fuel Element D3 in Core 176-AX1

For a given wire the C/E ratio is

$$(C/E)_i = NORM \times I_i(C) / I_i(E).$$

A fuel-element averaged C/E ratio is defined as $(C/E)_i$ averaged over all the wires in the fuel element.

The normalization constant depends only on those wires activated within standard fuel elements because only in these elements are precise wire locations known. Only one wire is activated in a fuel follower or a beryllium element and so no information regarding transverse gradients is available for these elements. Although attempts are made to place the wire in the central water channel of the fuel follower, it is impossible to see where the wire actually resides because of the configuration of the control rod. Also, the axial location of wires irradiated in the beryllium reflector elements is quite uncertain.

After aligning the measured peak activity with the calculated one or aligning axial reflector valleys for the fuel follower wires, axial integrations are performed and C/E ratios determined. However, these C/E ratios are subject to relatively large uncertainties because of wire position errors and because of the failure to account for any transverse gradients in these fuel followers and beryllium reflector elements.

The root-mean- square deviation (RMS-DEV) of the C/E ratios from unity provides an overall index of how well calculated and measured wire activity distributions agree. For reasons mentioned above, only those wires activated within standard 19-plate fuel elements are included in the evaluation of the RMS-DEV. Approximately two thirds of these C/E ratios differ from unity within the RMS-DEV value.

This wire analysis procedure together with some preliminary results is discussed in Ref. 26.

6.2 Differential and Integral Shim Rod Worths

As discussed in Section 2.3.1, control elements for the 30-MW Oak Ridge Research Reactor consist of square, water-filled, cadmium boxes 5.84 cm. on a side and 77.47 cm, long. The boxes are formed from a sheet of natural cadmium 0.1016 cm. thick which is clad with 0.0508 cm. thick aluminum.

Since the cadmium width-to-thickness ratio is much greater than unity, the control elements may be described by a set of thin slab absorbers for which spectrum- averaged group-dependent blackness coefficients (α,β) have been evaluated[22] in the P_5 approximation with scattering. In order to calculate control rod worths within the framework of normal diffusion theory, these blackness coefficients were used to obtain a set of effective diffusion parameters (D_{eff} and Σ_{aeff}) for the cadmium slabs as well as a set of internal boundary conditions (i.e. current-to-flux ratios) at the surface of the absorbers. These results, taken from Ref. 22, are summarized in Table 16. Since cadmium is such a strong absorber of thermal neutrons, it was found22 that cadmium rod worths could be accurately calculated by using the black internal boundary condition (j/φ = 0.4692) for group 5 (E_n < 0.625 eV) neutrons and normal diffusion theory for all the other groups. This is illustrated in Table 17 where the D6 integral rod worth in the ORR water-reflected fresh core 179AX5 is calculated using both VIM-Monte Carlo and DIF3D-diffusion codes with the cadmium represented by the group-5 black internal boundary condition in the diffusion calculation. The rod worth calculated by the two independent methods gives consistent results. Differential shim rod worths are calculated by determining the eigenvalues corresponding to the measured initial (R_i) and final (R_f) rod positions. Thus,

Table 16. Broad-Group Blackness Coefficients and Effective Diffusion Parameters for a 0.1016-cm-Thick Cadmium Slab

Quantity	Group 1	Group 2	Group 3	Group 4	Group 5
E_U(eV)	1.0E+07	8.208E+05	5.531E+03	1.855	0.6249
Σ_a/Σ_s	5.7044E-03	3.5980E-02	4.6885E-01	3.3797	2.7866E+02
$\Sigma_a\tau$	1.4074E-04	1.1472E-03	1.6371E-02	8.3122E-02	6.8515E+00
$<\alpha(P_5)>$	7.2304E-05	5.7371E-04	7.0560E-03	3.6251E-02	4.4449E-01
$<\beta(P_5)>$	2.6868E+01	2.0183E+01	1.3453E+01	8.6247E+00	4.7099E-01
$h=\tau$.					
D_{eff}	1.3649E+00	1.0253E+00	6.8343E-01	4.3814E-01	2.3926E-02
$\Sigma_{a\,eff}$	1.4233E-03	1.1294E-02	1.3897E-01	7.1662E-01	1.5556E+02
$h=\tau/2$:					
D_{eff}	1.3649E+00	1.0253E+00	6.8334E-01	4.3768E-01	1.4800E-02
$\Sigma_{a\,eff}$	1.4233E-03	1.1294E-02	1.3893E-01	7.1511E-01	3.6893E+01

*τ is the slab thickness (0.1016 cm) and h is the mesh interval width within the slab.

Table 17. Calculated D6 Integral Rod Worth for ORR Core 179AX5

Code	R_i. inch	R_f inch	Rod Bank inch	k_i	k_f	%δk/k
VIM	UL = 26.56	LL = 0.0	17.72	1.04001 ±0.00183	0.96663 ±0.00200	7.299 ±0.273
DIF3D	UL = 26.56	LL = 0.0	17.72	1.03714	0.96406	7.309

$$\% \, \delta \frac{k}{k} / \text{inch (calc.)} = 100 \; \left(\frac{1}{k_i} - \frac{1}{k_f}\right) / (R_f - R_i).$$

Normally, differential shim rod worths (%δk/k /inch) were measured in the ORR by the positive period technique. By waiting a sufficient length of time following the positive reactivity insertion, the transient terms die out so that the time-dependent flux approaches a pure exponential from which the asymptotic period is determined. The inhour equation relates this period to the reactivity, making use of delayed fission neutron parameters. However, preliminary analyses[27] showed 20 to 40% differences between measured and calculated differential shim rod worths in the ORR.

For a typical ORR core with partially burned fuel, intense gamma ray fields and associated photoneutron sources required that the reactor operate at a steady state power of about 3 kW before the start of a differential rod worth measurement. During the course of the measurement fluxes increase by factors as large as 75-100. Thus, at the end of the transient the reactor power may be well over 200 kW so that temperature changes in the fuel, clad and coolant are important. Under these conditions temperature- related feedback effects are present and so the time-dependent flux never approaches the shape of a pure exponential. This is the situation one encounters for control rod calibrations made in the ORR. Other reactivity measurements depend on this calibration data.

In an effort to overcome these difficulties, time-dependent flux profiles were measured following the positive reactivity insertions. A method was developed for extracting the asymptotic period from the shape of the initial part of the flux profile curve where transient terms are present but where fuel-moderator temperature changes are still negligible.

From measured time-dependent flux profiles, periods were determined at numerous times after the control rod displacement. Some typical results are given in Table 18 for core 179AX5. This table illustrates that feedback effects prevent the attainment of a pure asymptotic period.

The method used to extract the asymptotic period from the initial portion of the measured flux transient is based on the point kinetics model. For monoenergetic neutrons, the space-independent kinetic equations are

$$dn/dt = [k_{eff}(1-\beta) - 1]\,\frac{n}{l_p} + \sum_{i=1}^{m} \lambda_i C_i + S$$

$$dC_i/dt = k_{eff}\,\beta_i\,\frac{n}{l_p} - \lambda_i\,C_i$$

where

n = neutron density

l_p = prompt neutron lifetime

C_i = precursor concentration of ith delayed neutron group

λ_i = decay constant of the ith precursor

S = inherent neutron source strength in neutrons /cm^3 sec

Table 18. Period Measurements in ORR Core 179AX5
(Fresh Fuel, Water Reflected)

Rod D4		Rod D6		Rod F4		Rod F6	
R_i	12-00"	R_i	18.001,	R_i	18.00"	R_i	12.00"
R_f	12.23"	R_f	18.58"	R_f	18.89	R_f	12.23
Rod Bank	17.75"	Rod Bank	14.49"	Rod Bank	15.00"	Rod Bank	16.54"
TARM* sec	Period sec	TARM* see	Period sec	TARM* see	Period sec	TARM* sec	Period sec
34.0	45.14±0.34	29.6	44.21±0.38	38.4	68.72±0.84	24.0	50.65±0.56
34.6	45.18±0.33	35.8	45.62±0.32	58.4	69.21±0.67	41.8	53.40±0.35
34.6	τ^{**} = 42.9	35.8	τ^{**} = 43.4	58.4	τ^{**} = 68.3	41.8	τ^{**} = 51.2
54.0	47.55±0.27	49.6	46.21±0.31	78.4	71.92±0.64	44.0	52.90±0.50
74.0	48.50±0.23	69.6	48.44±0.30	98.4	73.00±0.66	64.0	53.57±0.40
94.0	51.26±0.22	89.6	51.15±0.21	118.4	73.95±0-59	84.0	55.09±0.36
114.0	54.72±0.25	109.6	53.83±0.22	138.4	76.98±0.54	104.0	58.32±0.30
		129.6	59.04±0.26	158.4	79.89±0.50	124.0	60.09±0.26
				178.4	83.33±0.50	144.0	64.79±0.34

*TARM = time after rod movement to middle of period measurement.
**τ = period measured with stop watch for flux to increase by a factor of e = 2.71828.

βi = effective delayed neutron fraction for the ith group

$$\beta \equiv \sum_{i=1}^{m} \beta_i = \text{ total delayed neutron fraction}$$

k_{eff} = effective multiplication factor

If the reactor operates at a steady state level no long enough to obtain saturated concentrations C_i of the delayed neutron precursors, the time-dependent flux following a step change in reactivity is given by

$$n(t)/n_o = \sum_{j=1}^{m+1} (A_j + B_j)\, e^{\omega_j t} + C$$

where the ω_j's are the (m+1) roots of the inhour equation,

$$\rho = \frac{l_p\, \omega + \omega \sum_{i=1}^{m} \beta_i/(\omega + \lambda_i)}{1 + l_p\, \omega} = \frac{k_{eff} - 1}{k_{eff}} ,$$

and where

$$A_j = \frac{(1-\rho)[l_p + k_o \sum_{i=1}^{m} \beta_i / (\omega_j + \lambda_i)]}{l_p (1-\rho) + \sum_{i=1}^{m} \beta_i \lambda_i / (\omega_j + \lambda_i)^2}$$

$$B_j = \frac{(1-\rho)(1-k_o)}{\omega_j [l_p (1-\rho) + \sum_{i=1}^{m} \beta_i \lambda_i / (\omega_j + \lambda_i)^2]}$$

$$C = (1 - 1/\rho)(1 - k_o) .$$

Note that k_0 is the initial value of k_{eff} prior to the step change in reactivity. Since at this time the reactor is in a steady state condition, $k_0 < 1$ if $S > 0$. From the original kinetic equations it follows
That

$$1 - k_o = l_p\, S / n_o .$$

The photoneutron source S builds up in a reactor due to long-lived fission product gamma activity associated with partially burned fuel elements. For measurements made in the ORR the steady state power level was large enough to have essentially infinite multiplication and thus be truly critical. Under these conditions $k_0 = 1$ and so the coefficients B_j and C vanish in the above

equations. The flux amplitudes A, are normalized so that $\Sigma A_j = 1.0$. For positive reactivities ($\rho>0$) all the roots of' the inhour equation are negative except one whose reciprocal is the asymptotic period.

To analyze the data one begins by calculating the flux ratio $n(t_2)/n(t_1)$ from the measured flux profile where t_2 and t_1, are the times after the reactivity step change. From an initial guess for the value of the asymptotic period, a preliminary value for the reactivity is obtained from the inhour equation. After writing this equation in polynomial form, the subroutine ZRPOLY from the International Mathematical and Statistical Libraries, Inc. (IMSL) calculates the zeros (ω_j) using the Jenkins-Traub three-stage algorithm described in Ref. 28. These values are then used in the above equations to calculate the flux ratio $n(t_2)/n(t_l)$. An iterative technique is followed whereby the value of the reactivity is adjusted until the calculated flux ratio agrees with the measured one. The asymptotic period is then just the reciprocal of the positive root corresponding to this reactivity. Using this procedure a program was developed to determine the reactivity, the asymptotic period, and the differential rod worth from the measured flux profile data. In principal, this method works equally well in the initial region of the flux profile where transient terms are present as well as in the asymptotic range where, if temperature changes are negligible, the time-dependent flux is a pure exponential. In practice, however, temperature changes are not negligible so that the flux ratio $n(t_2)/n(t_1)$ was evaluated near the beginning of the profile where perturbations from changing temperatures are still very small.

In the application of this technique to the measurement of differential shim rod worths, it is important to consider factors which limit the accuracy of the method. The more important of these factors are discussed below.

The accuracy of the reactivity determination is limited by the statistical uncertainty with which the $n(t_2)/n(t_1)$ flux ratio is measured. The greater the period the more sensitive are the results to this error. For example, for periods in the range from 40-45 seconds, a 1% error in the flux ratio leads to about a 1.25% error in the differential worth. However, for periods in the 80-90 second range, a 1% error in the flux ratio results in about a 3% error in the differential worth. Thus, periods longer than 60 seconds should be avoided if possible. Because of the sensitivity of the results to the measured flux ratio, corrections were applied for count losses associated with the detection equipment needed to record the time-dependent flux profile. A double pulser was used to measure the resolving time (1.5μsec) of the flux profile channel. This value was used for all the counting loss corrections.

The analytical solution to the point kinetic equations, upon which this technique is based, assumes that the reactivity insertion is instantaneous (i.e., a step function). In practice, however, the shim rod cannot be moved instantaneously from its initial position R_i to its final position Rf. The effect of the finite time for the rod movement on the kinetic response has been addressed by C. E. Cohn (Ref. 29) who assumed that p varies linearly in time as the rod moves from Ri to Rf. The effective instantaneous step change occurs at a time $T' < 0.5\ T$, where T is the time for the rod movement. As $\rho \rightarrow 0$, $T' \rightarrow 0.5\ T$. However, the flux predicted by the effective instantaneous step change is always somewhat less than the actual case. For the purpose of data analysis it is usually sufficient to set $T' = 0.5\ T$. The error introduced by this assumption becomes vanishingly small for large t_1 and t_2 sampling times. However, to minimize errors from temperature-related negative feedback effects, small sampling times are necessary. For $t_1 = 20.0$ see and $t_2 = 40.0$ sec, as measured with respect to the end of the shim rod movement, the error in the differential shim rod worth due to the uncertainty in T' is about 0.6%.

Differential shim rod worths depend on the actual displacement, R_f - R_i = ΔR, of the rod in question. In the ORR a digital readout system measures the rod positions to 0.01 inch. The accuracy relative to a fixed reference position is about 0.005 inch. For differential worth measurements rod displacements may be as small as 0.25 inch so that these measurement errors can result in about a 3% error in the measured reactivity.

The accuracy of the reactivity obtained from the shape of the measured flux profile ultimately depends on the accuracy with which the kinetic parameters (i.e., the λ_i, β_i set) are known. These matters are discussed in Section 6.3. Some errors in reactivity measurements due to photoneutron effects are examined in Ref. 30. For cores containing previously irradiated fuel delayed photoneutrons contribute to the kinetic response of the reactor to a positive reactivity insertion, resulting in a larger differential worth than would be the case if delayed photoneutrons were neglected.

6.3 Determination of Reactor Kinetic Parameters

To determine differential rod worths from measured time-dependent flux profiles, kinetic parameters (α_i, β_i) are needed in addition to a value for the prompt neutron lifetime, l_p. The prompt neutron lifetime was calculated for several ORR core configurations using the 1/v insertion method with ^{10}B chosen as the 1/v absorber. According to this technique the reactor is uniformly poisoned with a weak concentration of ^{10}B and the corresponding eigenvalue calculated. It follows that

$$\lim_{N \to 0} \; \delta \frac{k}{k} \; / \; N(^{10}B)\sigma_{ao} \, v_o = l_p$$

here N is the ^{10}B concentration (atoms / b-cm) and σ_{a0} is the neutron absorption cross section (barn) at speed v. (cm/sec). For v_0 = 2200 m/sec, σ_a = 3837 barns. δk / k is the worth of ^{10}B at concentration N.

Delayed fission neutron parameters were calculated as follows. Beginning with burnup-dependent cross sections, flux and adjoint distributions were calculated using the three-dimensional code, DIF3D. With these distributions as input, VAR13D calculations determined the effective delayed neutron fractions and the corresponding decay constants. The evaluated six-family coalesced set of the (λ_i,β_i) kinetic parameters is based on ENDF/B-V delayed neutron data. Values for the kinetic parameters determined in this manner are given in Table 19 for the water- and beryllium-reflected fresh LEU cores 179AX5 and 179AX6, respectively, and for core 179A. Figure 14 shows the configuration of each of these assemblies. For these cores calculated prompt neutron decay constants (β_{eff}/l_p) are compared with measured ones in Section 7.4.

Delayed photoneutrons arise from the $^9Be(\gamma y, n)$ reaction in the beryllium reflector and from the $^2H(\gamma,n)$ reaction in the water moderator. Because of many years of operation of the ORR at full power using recirculated water, the deuterium content in the moderator from (n,γ) reactions in hydrogen is considerably higher than what one might expect based only on natural abundance considerations. Plans to measure an effective set of kinetic parameters, including delayed photoneutrons, by the flux dieaway method[31] following a rod drop had to be abandoned when the ORR was unexpectedly and permanently shut down for reasons unrelated to the demonstration.

Table 19. Delayed Fission Neutron Parameters

Core	l_p μ-sec	Quantity	Group 1	Group 2	Group 3	Group 4	Group 5	Group 6	β_{eff}
179AX5	41.552	λ_I (SEC^{-1}):	1.2722E-2	3.1743E-1	1.1619E-1	3.1146E-1	1.4002E+0	3.8751E+0	
		$(\beta_{eff})_i$:	3.0436E-4	1.6940E-3	1.4926E-3	3.2461E-3	1.0305E-3	2.1204E-4	7.9795E-3
179AX6	76.520	λ_I (SEC^{-1}):	1.2722E-2	3.1743E-2	1.1617E-1	3.1142E-1	1.4002E+0	3.8746E+0	
		$(\beta_{eff})_i$:	3.0073E4	1.6746E-3	1.4756E-3	3.2080E-3	1.0176E-4	2.0914E4	7.8857E-3
179A	55.542	λ_I (SEC^{-1}):	1.2726E-2	3.1718E-2	1. 1658E-1	3.1196E-1	1.3990E+0	3.8547E+0	
		$(\beta_{eff})_i$:	2.7436E-4	1.5488E-3	1.3620E-3	2.9396E-3	9.3589E-4	1.9410E-4	7.2546E-3

	1	2	3	4	5	6	7	8	9
A									
B									MICRO MICRO AMP
C				F	F	F			
D			F	SR	F	SR	F		
E			F	F	F	F	F		
F	FC		F	SR	F	SR	F		FC
G									

Core 179AX5. Water-reflected critical with all fresh LEU fuel.

	1	2	3	4	5	6	7	8	9
A									
B									MICRO MICRO AMP
C		BE	BE	BE	BE	BE	BE	BE	
D		BE	BE	SR	F	SR	BE	BE	
E		BE	BE	F	F	F	BE	BE	
F	FC	BE	BE	SR	F	SR	BE	BE	FC
G		BE	BE	BE	BE	BE	BE	BE	

Core 179AX6. Beryllium-reflected critical with all fresh LEU fuel.

	1	2	3	4	5	6	7	8	9
A	DF	BE	N016	B082	N002	B083	B097	BE	DF
B	BE	BE	C036	U8003	B041	U8006	C037	BE	BE
C	BE	C035	NFE7J	B048	B042	B049	AL	N017	BE
D	BE	N020	B095	U8007	B043	U8008	B096	C031	BE
E	BE	B084	AL	B050	B044	C032	AL	B085	BE
F	BE	BE	N015	U8003	N013	U8004	N019	BE	BE
G	DF	BE	BE	BE	BE	BE	BE	BE	DF

Core 179AX7. Core used for measurements under high (18,000 gpm) and low (1200 gpm) flow rate conditions.

Fig. 14. ORR Core Configurations

The effective delayed neutron fraction, Off, may be written as

$$\beta_{eff} = \sum_{i=1}^{m} \gamma_i \beta_i (1 - \exp{-\lambda_i t_e}) + \sum_{j=1}^{n} \gamma_j \beta_j (1 - \exp{-\lambda_j t_e})$$

where the indices i and j refer to delayed fission neutrons and delayed photoneutrons, respectively. The factor (1-exp-λt_e)corrects for undersaturation precursor concentrations where t_e is the time interval during which the reactor is maintained at a steady power level prior to the reactivity transient. In so far as promoting fission is concerned, the effectiveness of delayed neutrons (γ_i ,γ_j) is different from that of prompt neutrons. This is because the delayed neutrons have a lower average energy than prompt neutrons resulting in fewer of them leaking out of the reactor. However, gamma energy degradation, absorption and leakage reduce the γ_j values. For t_e > 7 minutes, the above equation may be written in the form

$$\beta_{eff} = \sum_{i=1}^{m} \beta_{eff_1} + \bar{\gamma}_p (Be) \sum_{j=1}^{n} \beta_j (1 - \exp{-\lambda_j t_e}) + \bar{\gamma}_p (^2H) \sum_{k=1}^{km} \beta_k (1 - \exp{-\lambda_k t_e})$$

Photoneutron parameters for beryllium and deuterium are taken from Ref. 32 and are shown in Table 20. In the absence of experimental data, estimates for γ_p(Be) and γ_p (^{2}H) were obtained by requiring the average value of the C/E ratios for differential shim rod worths be approximately unity for cores 179AX3 and 179AX4 (see Fig. 14). These two cores are nearly identical and contain previously irradiated fuel. However, 179AX3 is beryllium-reflected whereas 179AX4 is water-reflected. This analysis yielded the values γ_p(Be) = 0.90 and γ_p(^{2}H) = 0.54 for the average effectiveness of delayed photoneutrons from beryllium and deuterium, respectively.

6.4 Cycle-Averaged Fuel Element Powers and ^{235}U Burnups From Gamma-Scanning Measurements on Full-Sized Fuel Elements

Following each irradiation cycle, the fuel elements were gamma scanned for the activity distribution to determine fuel element powers and burnups on a cycle-by-cycle basis. In addition, ^{137}Cs activity measurements on spent fuel elements were used to determine burnups integrated over all previous irradiation cycles. Methods for interpreting gamma scanning data from full-sized fuel elements are discussed below.

6.4.1 Methodology

The equations which govern the population densities of ^{140}Ba, ^{140}La, and ^{137}Cs during the irradiation cycle are:

$$dN_B / dt = Y_B F - \lambda_B N_B - \sigma_B \bar{\Phi} N_B$$

$$dN_L / dt = \lambda_B N_B - \lambda_L N_L - \sigma_L \bar{\Phi} N_L$$

$$dN_C / dt = Y_C F - \lambda_C N_C - \sigma_C \bar{\Phi} N_C$$

Here the subscripts B, L, and C refer to ^{140}Ba, ^{140}La, and ^{137}Cs, respectively. F is the cycle-averaged fission rate per unit volume and Y is the fission yield. In all cases neutron capture losses ($\sigma\varphi$) are negligibly small relative to the λ decay constants. These equations determine the specific activity of ^{140}La and ^{137}Cs at a given point **r** in the fuel. Thus, the ^{140}La specific activity, $A_L(\mathbf{r})$, may be written as

Table 20. Group Constants for Delayed Photoneutrons from ^{235}U Fission Gammas on Be and D_2O*

Group Index, i	Beryllium $\lambda_i(sec^{-1})$	Beryllium $\beta_i(10^{-5})$	Deuterium $\lambda_i(sec^{-1})$	Deuterium $\beta_i(10^{-5})$
1	6.24E-7	0.057	6.26E-7	0.05
2	2.48E-6	0.038	3.6313-6	0.103
3	1.59E-5	0.260	4.37E-5	0.323
4	6.20E-5	3.20	1.17E-4	2.34
5	2.67E-4	0.36	4.28E-4	2.07
6	7.42E-4	3.68	1.50E-3	3.36
7	3.60E-3	1.85	4.81E-3	7.00
8	8.85E-3	3.66	1.69E-2	20.4
9	2.26E-2	2.07	2.77E-1	65.1
Total		15.175		100.75
Ave. Photoneutron Lifetime $=\Sigma(\beta_i/\lambda_i)\Sigma\beta_i$:		3.33 hr.		24.1 min.

*Data taken from Ref 32.

$$A_L(\mathbf{r}) = Y_B\, F(\mathbf{r})\, BDF_L(\mathbf{r}) = CR_L(\mathbf{r}) / V_S E_L\,, \tag{1}$$

where $BDF_L(r)$ is the buildup-decay factor for ^{140}La and is given by

$$BDF_L = \sum_{i=1}^{m} \frac{\lambda_L\,(1-\exp{-\lambda_B t_{ei}})\exp{-\lambda_B t_{wi}} - \lambda_B\,(1-\exp{-\lambda_L t_{ei}})\exp{-\lambda_L t_{wi}}}{\lambda_L - \lambda_B}\,. \tag{2}$$

Here, in is the number of reactor startups for a given irradiation cycle, t_{ei} is the exposure time (in equivalent full-power days for the ith startup, and t_{wi} is the wait interval (days) from the ith reactor shutdown until the ^{140}La activity is counted. The values for t_{ei} and t_{wi} are obtained from the count times and the detailed power histories for each irradiation cycle. In Eq. (1) $CR_L(r)$ is the observed count rate associated with the decay of ^{140}La and is corrected for a residual activity from earlier irradiation cycles. EL is the probability that a ^{140}La decay occurring in the volume V_s "seen" by the detector will result in a registered count. It follows from Eq. (1) that the residual ^{140}La count rate at time t_c, $RCR_L(t_c)$, after n irradiation cycles is

$$RCR_L(t_c) = \sum_{i=1}^{n-1} CR_L(t_{ci})\,\frac{BDF_L(t_c)}{BDF_L(t_{ci})}\,\frac{RE(t_{ci})}{RE(t_c)} \tag{3}$$

where $RE(t_c)$ is the relative efficiency of the detector system at time t_c. These relative efficiency factors account for possible long term changes in detector efficiency and were measured by periodically counting the ^{137}Cs activity of fuel element C021. Note that the net count rate in Eq. (1) has been normalized (divided) by the appropriate relative efficiency factor.

The fuel element power and burnup depend on the total fission rate in the fuel element, which is the volume integral of the fission density. Thus,

$$\int F(\mathbf{r})d\mathbf{r} = V_M \langle F\rangle = \langle CR_L / BDF_L\rangle / Y_B G_L \tag{4}$$

where the overall geometric efficiency $G_L = (V_s / V_m)EL$. V_m is the volume of the fuel meat in the element and $\langle F\rangle$ is the volume-averaged fission density. If transverse gradients are negligible or are neglected, $\langle CR_L / BDF_L\rangle$ may be evaluated by numerically integrating the axial count rates divided by the corresponding values of BDF_L. It follows from this last equation that the total fissions which occurred in the fuel element during the irradiation cycle is

$$N_F(La) = \sum_{i=1}^{m} \langle CR_L / BDF_L\rangle_i\, t_{ei} / Y_B\, G_L. \tag{5}$$

Because of the 30.17 year half life of ^{137}CS, the specific cesium activity, $A_c(r)$, is directly related to the total fission density, TF.

$$A_C(\mathbf{r}) = Y_C\, \lambda_C\, TF(\mathbf{r})\, BDF_C(\mathbf{r}) = CR_C(\mathbf{r}) / V_S\, E_C \tag{6}$$

where the subscript C is used to denote ^{137}Cs quantities and where the buildup-decay factor (BDF) is given by

$$BDF_C(\mathbf{r}) = \sum_{j=1}^{n} F(\mathbf{r})_j[1-\exp(-\lambda_C\, t_{ej})]\exp(-\lambda_C\, t_{wj}) / \lambda_C \sum_{j=1}^{n} F(\mathbf{r})_j\, t_{ej}$$

$$\approx \sum_{j=1}^{n} t_{ej} \exp(-\lambda_C t_{wj}) / \sum_{j=1}^{n} t_{ej} \tag{7}$$

In Eq. (7) n is the number of irradiation cycles during which the fuel element was activated. As for the case of ^{140}La, CRC in Eq. (6) is the measured ^{137}Cs count rate divided by the appropriate relative efficiency factor. The total number of fissions which occurred in the discharged fuel element, $N_F(C_S)$ is given by the volume integral of TF(r).

$$N_F(Cs) = \int_{fuel} TF(r)\, dr = V_M \langle TF \rangle = \langle CR_C / BDF_C \rangle / \lambda_C\, Y_C\, G_C \tag{8}$$

where $G_c (V_s / V_m) E_c$ is the overall geometric efficiency factor for the detection of ^{137}Cs gamma rays. If the effects of transverse gradients are negligible, $\langle CR_c / BDF_c \rangle$ may be evaluated by numerically integrating the axial distribution of ^{137}Cs count rates divided by the appropriate value of BDF_c.

The fuel element cycle-averaged power (P) is directly proportional to the total fission rate.

$$\bar{P}(MW) = V_M \langle F \rangle E_R = E_R \langle CR_L / BDF_L \rangle / Y_B\, G_L \tag{9}$$

E_R is the recoverable energy per fission and has a value of 3.152E-17 MW-sec/fiss for the thermal fission of ^{235}U and the subscript L refers to ^{140}La quantities.

The ^{235}U burnup depends on the total number of fissions, N_F., which occurred in the fuel element. Thus,

$$\Delta\, {}^{235}M = (1 + {}^{235}\bar{\alpha})\, N_F\, ({}^{235}F / F)\, {}^{235}AW / N_A \tag{10}$$

where 235α is the spectrum-averaged ^{235}U capture-to-fission ratio, ^{235}F/F the fraction of fissions due to ^{235}U, Δ^{235}W the atomic weight of ^{235}U, and NA is Avogadro's number. Because 235 U and 235F/F vary somewhat as a function of burnup, Δ^{235}W was obtained from a least squares polynomial fit of the form

$$\Delta\, {}^{235}M = \sum_{i=1}^{6} a_i N_F^{i-1}. \tag{11}$$

REBUS3 -calculated values for Δ^{235}W and N_F. over a wide range of burnups were used to determine the a_i fitting coefficients for both HEU and LEU fuel.

Once the effective geometric efficiency factors, G_L and G_C, are known, Eqs. (9) and (11) determine the fuel element power and burnup. Small corrections for power density gradients transverse to the fuel element axis will be discussed in section 6.4.3.

6.4.2 Calibration of the Gamma-Scanning System

The effective geometric efficiency, G,,, of the gamma-scanning system for the detection of the ^{140}La 1.586 MeV line is different for HEU and LEU fuel. This is because the self-attenuation of gamma rays within the fuel element depends on the uranium density, which is substantially larger in the LEU than in the HEU fuel. The calibration procedure relies on the fact that during each cycle the ORR operated at a power level of 30 MW, a power frequently determined by heat balance measurements. This total reactor power is shared among the HEU and LEU fuel elements in the core, the fuel followers, and the mini-plates in the HFED test rig. Following the notation used in the last section, the total power developed in the HEU and LEU fuel elements is

$$30(1 - PF_{FF}) = \sum_{i=1}^{m} P_i(HEU) + \sum_{j=1}^{n} P_j(LEU)$$

$$= \frac{E_R}{Y_B G_L\,(HEU)} \sum_{i=1}^{m} \langle CR_L / BDF_L \rangle_i + \frac{E_R}{Y_B G_L\,(LEU)} \sum_{j=1}^{n} \langle CR_L / BDF_L \rangle_j$$

where m and n are the number of HEU and LEU fuel elements in the core, respectively, and where

PF_{FF}	=	the power fraction developed in the fuel followers and the mini
	=	fuel plates.
E_R	=	the recoverable energy per fission event.
Y_B	=	the total fission yield for the $^{140}Ba \rightarrow {}^{140}La$ chain.
G_L	=	the effective geometric efficiency for the detection of the 1.596 MeV ^{140}La gamma ray.
$\langle CR_L / BDF_L \rangle$	=	the position-dependent ^{140}La count rate (CR_L) adjusted by the radioactivity buildup and decay factor (BDF_L) for the $^{140}Ba \rightarrow {}^{140}La$ chain, and averaged over the height of the fuel column.

Although they could have been included in the definition of G_L, literature values were used for E_R and Y_B. The fuel followers, which formed the lower portion of the shim rod assemblies, were used in successive cores until final burnup was achieved. For this reason and because of their special geometry they were not gamma-scanned on a cycle-by-cycle basis. Therefore, a calculated value for the power fraction P_{FF}, which comes almost entirely from fuel follower contributions, has to be used. Typical values for P_{FF} range from about 0.10 to 0.15.

An equation of the above type was written for each of the 13 mixed cores used in the ORR demonstration during the transition from an all-HEU to an all-LEU core. Using the gamma-scanning data and applying the method of least squares to these 13 equations determined values for G_L(HEU) and G_L(LEU) . The results are

$$G_L(HEU) = (4.161 \pm 0.073)\ \ 10^{-13}$$

$$G_L(LEU) = (3.961 \pm 0.072)\ \ 10^{-13}\ .$$

The LEU result is in good agreement with the value based on the seven all-LEU cores reported in Ref. (33), namely

$$G_L(\text{LEU}) = (3.944 \pm 0.030)\ 10^{-13}\ .$$

For a given fuel element the accumulated total fissions obtained from ^{140}La counting data must equal that obtained from the ^{137}Cs data. This fact allows a determination of the effective geometric efficiency ratio $G_C(^{137}\text{Cs}) / G_L(^{140}\text{La})$ for each fuel element whose entire irradiation history occurred during the ORR demonstration. From Eqs. (5) and (8) in section 6.4.1 it follows that

$$G_C(^{137}\text{Cs}) / G_L(^{140}\text{La}) = \frac{\langle CR_C / BDF_C \rangle / \lambda_C Y_C}{\sum_{i=1}^{n} \langle CR_L / BDF_L \rangle_i\, t_{ei} / Y_B}$$

where the summation extends over the n irradiation cycles of length t_{ei} . Averaging these ratios for the three HEU and 68 LEU fuel elements first irradiated during the ORR whole-core demonstration and combining them with the above G_L values gives the following results for the ^{137}Cs effective geometric efficiencies:

$$G_C(\text{HEU}) = (3.395 \pm 0.067)\ 10^{-12}$$

$$G_C(\text{LEU}) = (2.937 \pm 0.023)\ 10^{-12}\ .$$

At the end of the ORR demonstration the LEU shim rods were cut to remove the lower fuel follower section from the upper cadmium poison section. In order to determine their final burnup status, these fuel followers were gamma-scanned for ^{137}Cs. Because of differences in uranium densities, the above value for G_c(LEU) needs to be adjusted for the case of the LEU fuel followers. For an homogenized fuel slab with a uniform distribution of fission product gamma ray sources the fraction of gamma rays escaping without attenuation, FE, is

$$F_E = [1 - \exp(-\mu t)] / \mu t$$

where t is the homogenized slab thickness and R the energy-dependent gamma ray attenuation coefficient. Using data from Ref. (34), the ^{137}Cs 0.662 MeV gamma ray escape probability from the 15-plate LEU fuel followers relative to the 19-plate LEU standard fuel elements was calculated to be 1.0622. Combining this with the above value for G_c(LEU) gives an effective geometric efficiency for the LEU fuel followers of

$$G_C(\text{LEU-FF}) = (3.120 \pm 0.040)\ 10^{-12}\ .$$

6.4.3 Transverse Gradient Corrections

Up to this point die analysis of the gamma-scanning data was based on the assumption that fission rate gradients in directions transverse to the fuel element axis were negligibly small. A method35 for calculating transverse gradient correction factors has been developed with results applied to all of the demonstration cores.

Figure 15 shows the cross section of an ORR fuel element, defines the coordinate system used in the analysis, and indicates the detector location relative to the fuel element. For a given

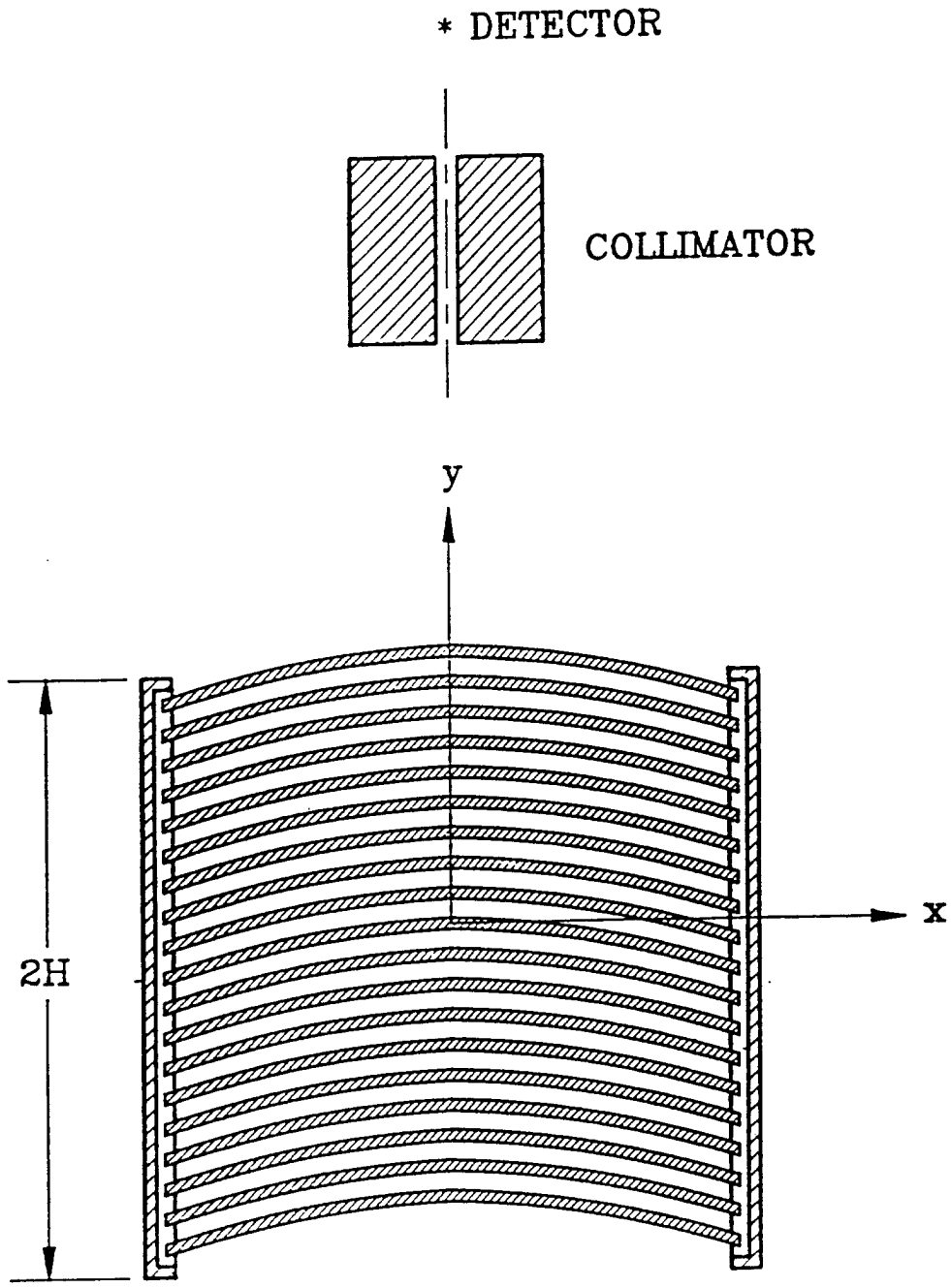

Fig. 15. Coordinate System for Calculating Transverse Gradient Correction Factors

axial location (z) the observed count rate is

$$CR(z) = C \int_{-H}^{H} PD(0,y,z) \exp[-\mu(H-y)]\, dy .$$

where

PD(0,Y,z)	=	the power density distribution in the fuel element along the y-axis at elevation z.
H	=	the half-thickness of the fuel element in the y-direction.
μ	=	the attenuation coefficient in the homogenized fuel composition for ^{140}La 1.596 MeV gamma rays. Gamma ray cross sections given in Ref. (34) were used to calculate g.
C	=	a proportionality constant.

If one neglects transverse gradients and equates the power density to the value averaged over xy plane of the fuel element the observed count rate would be

$$CR_{\overline{xy}}(z) = C\, PD_{\overline{xy}}(z) \int_{-H}^{H} \exp[-\mu(H-y)]\, dy .$$

The gradient correction factor (GCF) is given by the ratio of these count rates.

$$GCF(z) = CR_{\overline{xy}}(z) / CR(z)$$

To evaluate the GCFs it is convenient to express the power density along the y-axis in terms of a polynomial expansion.

$$PD(0,y,z) = PD_0(0,0,z)\, [1 + a_1 y + a_2 y^2 + \cdots + a_n y^n + \cdots]$$

From this it follows that the gradient correction factor GCF may be written as

$$GCF(z) = \frac{PD_{\overline{xy}}(z) / PD_0(z)}{1 + a_1 T_1 + a_2 T_2 + \cdots + a_n T_n + \cdots}$$

where

$$T_1 = [\mu H \coth(\mu H) - 1] / \mu$$

and where for n > 1,

$$T_n = H^n - n\, T_{n-1} / \mu \qquad \text{for even } n$$

$$T_n = H^n \coth(\mu H) - n\, T_{n-1} / \mu \qquad \text{for odd } n .$$

In most cases the expansion coefficients (a_n) were evaluated through sixth order using the mesh-centered power density file obtained from the output of the REBUS-3 burnup calculation. For each fuel element in the core and for each axial mesh interval throughout the height of the fuel column PD(0,y,z) was fit to a high degree polynomial by the least squares method. From these fits the a_n's were determined. The power density file was also used to determine the ratio $PD_{xy}(z) / PD_O(z)$. Thus, gradient correction factors were evaluated for each fuel element and for each axial mesh interval in the core. Since the axial variation of the GCF's was found to be small, an average value for each fuel element was obtained using the central power density, $PD_0(z)$, as a weighting function.

Finally, the fuel element averaged GCFs had to be normalized so as not to change the G_L -values discussed in the last section. This condition requires that

$$N \sum_{i=1}^{n} \langle GCF \rangle_i P_i = \sum_{i=1}^{n} P_i$$

where N is the normalization constant, $\langle GCF \rangle_i$ the gradient correction factor averaged over the height of the ith fuel element, P_i the fuel element power, and n the number of fuel elements in the core. For the ith fuel element,

$$\langle GCF \rangle = \int_0^{H_o} GCF(z)\, PD_0(z)\, dz \Big/ \int_0^{H_o} PD_0(z)\, dz$$

where H_o is the height of the fuel column.

Normalized transverse gradient correction factors for fuel elements in core 174D are tabulated in Fig. 16 together with estimated errors in the calculation. These error estimates are based only on the errors of the coefficients obtained from the least squares polynomial fits. Fig. 17 shows how the calculated-to-experiment (C/E) power ratios are influenced by the normalized gradient correction factors. The root-mean-square (RMS) value for the C/E deviations from unity is 0.051 without the application of the GCFs and 0.048 with the use of the GCFs. Thus, the application of transverse gradient correction factors only marginally improves the fuel element power C/E ratios. The RMS values suggest that about 68% of the fuel elements have C/E ratios that differ from unity by 5% or less and that 95% of the C/E ratios should be within 10% of unity. Results given in Fig. 17 are consistent with this interpretation. Appendix C provides a table of calculated transverse gradient correction factors for all of the ORR cores operated at 30 MW during the whole-core demonstration.

6.4.4 Interpretation of Fuel Follower Gamma-Scanning Measurements Made with a NaI Detector

At the end of the ORR whole-core demonstration the LEU fuel followers were gamma-scanned for ^{137}CS in order to measure their final burnup status. After data had been obtained for four of the eight LEU fuel followers the Ge(Li) detector failed. This detector could not be repaired or replaced before the fuel followers were to be shipped to Savannah River for reprocessing. Therefore, the eight LEU fuel followers were gamma-scanned with a standard 3" x 3" NaI detector.

Relative to the Ge(Li) detector, the resolution of the 3" x 3" NaI crystal was very poor so that many of the gamma ray peaks overlapped in the observed NaI spectrum. This made it very difficult to isolate the 0.662 MeV ^{137}Cs activities from the measured NaI spectra. Based on calculations using the ORIGEN code[36] and on spectra measured previously with the Ge(Li)

ORR CORE 174D
Transverse Gradient Correction Factors

	1	2	3	4	5	6	7	8	9
A	Be	1.006 ±0.001	1.034 ±0.001	1.016 ±0.002	0.991 ±0.002	1.016 ±0.002	1.040 ±0.002	1.010 ±0.001	Be
B	Be	Be	0.970 ±0.002	SR	0.975 ±0.001	SR	0.987 ±0.001	Be	Be
C	Be	1.011 ±0.002	MFE	1.004 ±0.001	0.974 ±0.000	0.992 ±0.001	MFE	0.998 ±0.002	Be
D	Eu	0.980 ±0.002	1.013 ±0.003	SR	0.972 ±0.001	SR	0.988 ±0.001	0.982 ±0.002	Eu
E	Be	0.986 ±0.000	HFED	0.993 ±0.001	Ir	1.007 ±0.001	Ir	1.018 ±0.001	Be
F	Eu	Be	1.013 ±0.001	SR	1.029 ±0.002	SR	1.019 ±0.002	Be	Eu
G	Be	Be	Be	Be	Be	Be	Be	Be	Be

N

E

SR = Shim Rod Assemblies

MFE = Magnetic Fusion Experiment

Ir, Eu = Irradiation Facility for Activating Iridium or Europium Samples

HFED = High U-load Fuel Element Device for Mini-Plate Irradiations

Be = Beryllium Reflector Element

= LEU Fuel Element

Fig. 16

ORR CORE 174D
Cycle-Averaged Power C/E Ratios

	1	2	3	4	5	6	7	8	9
A	Be	1.015 1.009	1.026 0.991	1.022 1.006	1.087 1.097	1.046 1.029	1.030 0.990	0.994 0.984	Be
B	Be	Be	0.973 1.003	SR	1.020 1.046	SR	0.950 0.962	Be	Be
C	Be	1.049 1.038	MFE	0.992 0.987	0.930 0.956	0.937 0.945	MFE	0.913 0.915	Be
D	Eu	0.973 0.993	0.997 0.984	SR	0.938 0.965	SR	0.910 0.921	0.903 0.920	Eu
E	Be	0.975 0.989	HFED	0.974 0.980	Ir	0.957 0.950	Ir	0.940 0.924	Be
F	Eu	Be	0.951 0.939	SR	0.995 0.967	SR	0.927 0.909	Be	Eu
G	Be	Be	Be	Be	Be	Be	Be	Be	Be

Without GCF's
With GCF's

N

E

SR = Shim Rod Assemblies

MFE = Magnetic Fusion Experiment

Ir, Eu = Irradiation Facility for Activating Iridium or Europium Samples

HFED = High U-load Fuel Element Device for Mini-Plate Irradiations

Be = Beryllium Reflector Element

= LEU Fuel Element

Fig. 17

detector before it failed, it was determined that the observed NaI spectra consisted of the superposition of twelve distinct gamma ray lines. These gamma rays and their known properties[37] are summarized in Table 2 1.

It was assumed that the observed NaI gamma ray spectra could be represented by a background function plus a series of twelve Gaussian functions, one for each of the gamma ray lines shown in Table 21. A 5th-degree polynomial was used to represent the continuous Compton distribution on the low-energy side of each of the full energy peaks. Thus, the assumed functional form of the measured spectrum is

$$y(x) = BKG(x) + \sum_{i=1}^{12} a_i \exp[-(x - p_i)^2 / 2w_i^2]$$

where

$$BKG(x) = \sum_{j=1}^{5} b_j x^{j-1}$$

The parameters a,, pi and w_i are the amplitude, peak location and the width parameter for the ith Gaussian. These parameters determine the area under the Gaussian and the full width at half maximum (FWHM) of the peak. Thus,

$$Area_i = a_i w_i [2\pi]^{1/2}$$

$$FWHM_i = 2 w_i [2 \ln 2]^{1/2}$$

The variable x in the above equations corresponds to the channel numbers of the observed pulse-height distribution, y(x).

Because of the poor resolution of the NaI detector, not all the parameters in the fitting function were regarded as independent. From the fitted locations of the principal gamma ray lines (511.865, 604.710, 661.660 and 795.867 keV), the calibration of the energy scale is determined from which the locations of the remaining lines are obtained. R. L. Heath's data[38], taken with a 3" x 3" NaI detector, was used to determine energy-dependent peak widths relative to that of the 661.660 keV ^{137}Cs line. Finally, the absolute gamma-ray yields shown in Table 21 were used to determine relative gamma-ray intensities for a given isotope. Relative Gaussian amplitude parameters were chosen in such a way that the ratio of peak areas preserved the relative gamma-ray intensities. Furthermore, the intensities of the ^{95}Zr lines relative to the 95Nb gamma ray were calculated from the irradiation and decay history of the fuel followers together with the absolute gamma ray yields in Table 21. Because of its low intensity, a calculation was also made relating the intensity of the 696.5 keV ^{144}Pr line to the ^{137}Cs gamma-ray.

In this way 27 of the parameters in the above fitting function were expressed in terms of 14 independent parameters, which are listed in Table 22. A non-linear least squares method, based on the Lavenberg-Marquardt algorithm[39] was used to adjust the 14 parameters so as to minimize the sum of the squares of the differences between the measured and calculated ordinates of the NaI gamma-ray pulse height distribution. The results from this least squares fitting process were used to determine position-dependent count rates associated with the ^{137}Cs activities. Figure 18 shows a typical comparison of a measured and a fitted NaI spectrum.

Table 21. Some Properties of the Twelve Gamma Ray Lines which Contribute to the Observed NaI Spectra[1]

Isotope	Production[2]	$T_{1/2}$	E_γ - keV	Absolute Yield, %
^{106}Rh	Parent: ^{106}Ru	1.020 y		
	Daughter: ^{106}Rh	29.80s	511.865	20.7
			621.920	9.8
^{134}Cs	^{133}Cs(n,γ)	2.062 y	563.237	8.38
			569.321	15.4
			604.710	97.6
			795.867	85.4
			801.951	8.73
^{137}Cs	Parent: ^{137}Xe	3.818 m		
	Daughter: ^{137}CS	30.0 y	661.660	85.21
^{144}Pr	Parent: ^{144}Ce	284.9 d		
	Daughter: ^{144}Pr	17.28 m	696.543	1.34
^{95}Nb	Parent: ^{95}Y	10.3 m		
	Daughter: ^{95}Zr	64.02 d	724.199	44.1
			756.729	54.5
	Daughter: ^{95}Nb	34.97 d	765.789	99.79

[1]Data taken from Edgardo Browne, et al., Table of Radioactive Isotopes Wiley, 1986.

[2]All the isotopes are produced as fission products except '34 Cs, which results from neutron capture on the stable fission product isotope "Cs.

Table 22. The 14 Independently Adjusted Parameters Used in the Non-Linear Least Squares Fitting Process for NaI Spectra

Quantity	Eγ - keV	Parameters
BKG(x)		b_l,b_2,b_3,b_4,b_5
^{106}Rh	511.865	a,p
^{134}CS	604.710	a,p
	795.867	p
^{137}Cs	661.660	a,p,w
^{95}Nb	765.789	a

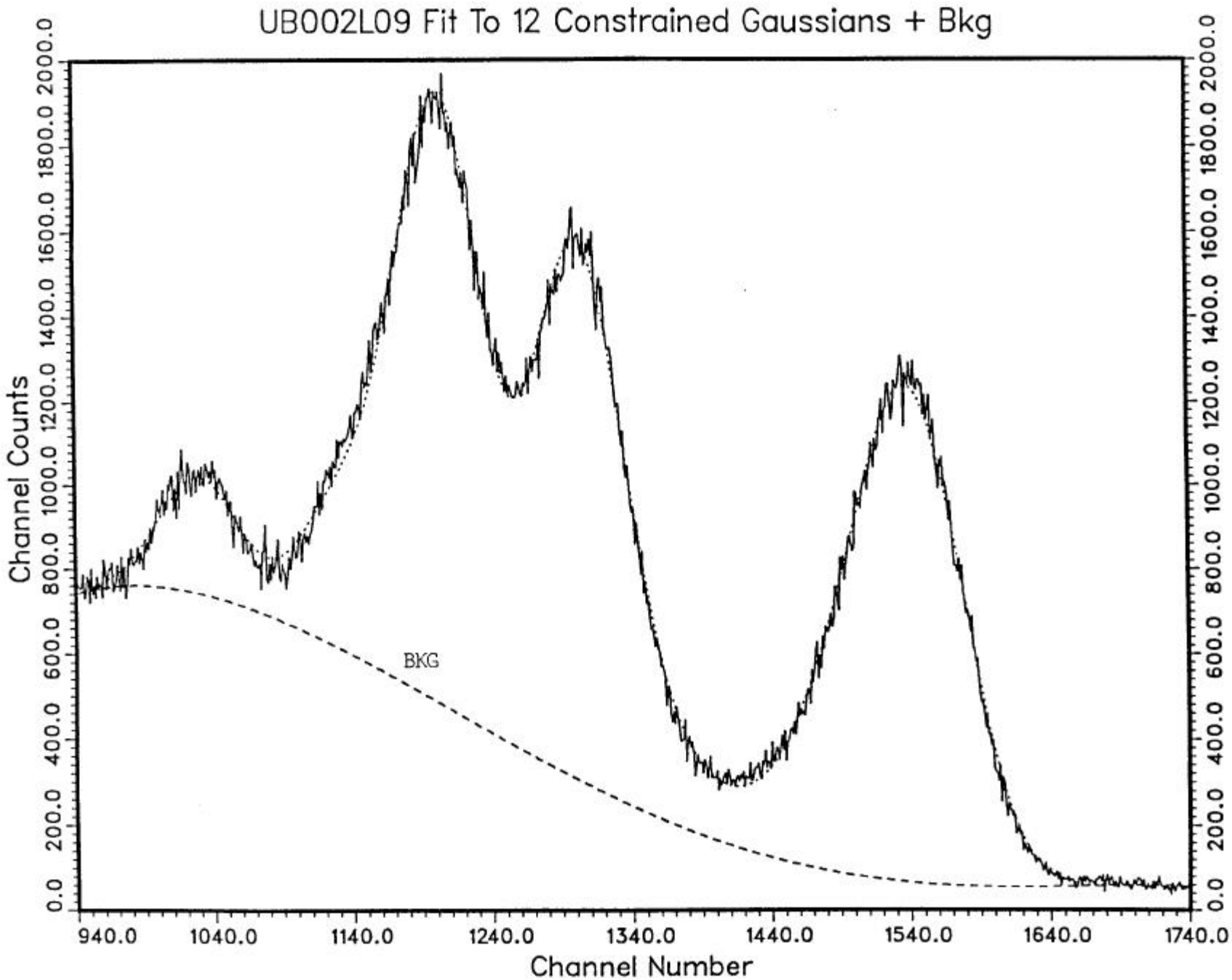
UB002L09 Fit To 12 Constrained Gaussians + Bkg
Channel Counts
0.0
200.0
400.0
600.0
800.0
1000.0
1200.0
1400.0
1600.0
1800.0
2000.0
BKG
940.0
1040.0
1140.0
1240.0
1340.0
1440.0
1540.0
1640.0
1740.0
Channel Number

Fig. 18

The efficiency of the NaI system for the detection of the 137Cs gamma ray relative to the Ge(Li) system was obtained from the four LEU fuel followers which were analyzed on both systems. This relative efficiency was found to have the value of 2.876 ± 0.023. Thus, the effective geometric efficiency factor for the NaI detection system for the measurement of ^{137}Cs activities in the LEU fuel followers is

$$G_C\,(NaI)_{LEU\,FF} = (8.97 \pm 0.14)\ 10^{-12}\ .$$

6.5 Fuel Element Burnups from Post-Irradiation Mass Spectrometry Measurements

At the end of the ORR whole-core demonstration a number of plates were removed from selected fuel elements and fuel followers and gamma-scanned in ORNL hot cells to measure ^{137}Cs activity distributions. In addition, samples for mass spectrometry analyses were cut from some of these plates. Analysis of this postirradiation data provides fuel-element-averaged ^{235}U burnups which are independent of those obtained from the gamma-scanning data of full-sized fuel elements.

For these plate measurements the gamma-scanning system consisted of a Ge(Li) detector and a collimator 17 inches long with a 0.125-inch-diameter circular aperture. Plates were scanned with the convex side facing the collimator. Table 23 list the plates which were gamma-scanned. Longitudinal scans were made along the plate centerline at the positions (relative to the top of the plate) listed in Table 24. Transverse scans were measured 14.8 inches from the top of the plate at the five positions shown in Table 25. Plates are numbered with respect to the top plate in Fig. 2. Mass spectrometer samples were cut from these plates as described in Table 26.

Pointwise ^{235}U burnups were obtained from the measured uranium mass spectra data. The equations for the uranium atom densities in fresh (denoted by a zero subscript) and burned fuel are

$$N = {}^4N + {}^5N + {}^6N + {}^8N = N_0 - (\,\Delta N^4 + \Delta N^5 + \Delta N^6 + \Delta N^8\,)$$

$$= N_0 - (1 + C + D + E)\ B\ {}^5N_0$$

where

$$\Delta N^5 = {}^5N_0 - {}^5N\ ,\ C = \Delta N^8 / \Delta N^5\ ,\ D = \Delta N^6 / \Delta N^5\ ,\ E = \Delta N^4 / \Delta N^5$$

$$B = {}^{235}BU = \Delta N^5 / {}^5N_0$$

Thus,

$$B = 1 - {}^5N / {}^5N_0 = 1 - N\,A / N_0\,A_0 = 1 - A / A_0\,[\ 1 - (\ 1 + C + D + E\ )\ B\ A_0\ ]\ .$$

Rearranging,

$$B = \frac{1 - A/A_0}{1 - (\ 1 + C + D + E\ )\ A}$$

where A_0 and A are the measured ^{235}U atomic abundances in fresh and burned fuel, respectively.
The small correction factors (C, D and E) may be evaluated from an EPRI-CELL burnup calculation. However, the results for LEU fuel arc quite insensitive to the calculated value for the sum (C + D + E). For burnups between 33 and 88% in LEU fuel C ranges from 0.12 to 0.18, D from -0.17 to -0.15, and E = 0.003.

Table 23. Gamma Scanning of ORR Fuel Plates

Fuel Element Ident.	Plate Position in Fuel Element*	Longitudinal Scan (No. of Points)	Transverse Scan (No. of Points)
B-043	2	16	5
	6	6	
	10	16	5
	14	6	
	18	6	
C-024	2	16	
	6	6	
	10	6	
	14	6	
	18	6	
N-007	2	16	
	6	6	
	10	6	
	14	6	
	18	6	
B-041	2	6	
C-025	2	6	
N-006	2	6	
T-490	2	16	
UB-002	2	16	5
	5	6	
	8	16	5
	11	6	
	14	6	
UB-005	2	16	5
	5	6	
	8	6	5
	14	6	

Plates are numbered with respect to the top plate shown in Fig. 2

Table 24. Measurement Points for Axial Gamma Scans

Point No.	Distance from Top of Plate (in.)
1	0.8
2	1.8
3*	2.8
4	4.8
5*	6.8
6	8.8
7*	10.8
8	12.8
9*	14.8
10	15.8
11	16.8
12*	18.8
13	20.8
14	21.8
15*	22.8
16	23.8

*Six points for abbreviated scan.

Table 25. Measurement Points for Transverse Gamma Scans

Point No.	Distance from Axial Centerline of Plate (in.)*
1	-0.9
2	-0.5
3	0.0
4	0.5
5	0.9

*Measured 14.8 in. from top of plate.

Table 26. Sections for Mass Spectrometry Samples

Fuel Element Ident.	Plate Position in Element	First Section Cuts (in. from top) From	First Section Cuts (in. from top) To	Second Section Cuts (in. from top) From	Second Section Cuts (in. from top) To
B-043	2	3.8	4.3	15.8	16.3
	10	15.8	16.3		
C-024	2	3.8	4.3	15.8	16.3
	10	15.8	16.3		
N-007	2	3.8	4.3	15.8	16.3
	10	15.8	16.3		
B-041	2	15.8	16.3		
C-025	2	15.8	16.3		
N-006	2	15.8	16.3		
T-490	2*	3.8	4.3	8.8	9.3
		15.8	16.3	20.8	21.3
UB-002	2	6.3	6.8	20.3	20.8
	8	6.3	6.8		
UB-005	2	4.8	5.3		
	8	4.8	5.3		

*Four sections removed from this plate.

The ^{137}Cs gamma-scanning data were used to relate the pointwise burnup values to the burnup averaged over the entire fuel element. Plate-averaged ^{137}Cs activities (^{137}A) were obtained by numerically integrating the axial and transverse distributions. Thus,

$$<^{137}A>_{plate} = \frac{\int_{x_L}^{x_U}\int_{z_L}^{z_U} {}^{137}A(x,z)\,dx\,dz}{(x_U - x_L)(z_U - z_L)}$$

$$\approx \frac{A(0,z_0)^{-1}\int_{x_L}^{x_U} A(x,z_0)\,dx \int_{z_L}^{z_U} A(0,z)\,dz}{(x_U - x_L)(z_U - z_L)}$$

Here the assumption is made that the transverse activity distribution, which is nearly constant, is independent of z. These integrals were evaluated numerically using both Simpson's Rule and trapezoidal methods. Values for the integration limits (in inches) are summarized below.

Fuel Element	L	L	L	L
19-plate standard	-1.24	+1.24	0.50	24.13
15-plate follower	-1.24	+1.24	0.45	23.30

Finally, fuel-element-averaged ^{137}Cs activities were obtained by numerically integrating the plate-averaged results over the number of plates in the fuel element. Thus,

$$<^{137}A>_{FE} = \frac{1}{N_p}\int_0^{N_p} <^{137}A(N)>_{plate}\,dN$$

where N_p is the number of plates in the element.

The fuel-element-averaged burnup may now be written as

$$<BU> = \frac{<^{137}A>_{FE}}{^{137}A(x,y,z)}\,BU(x,y,z)$$

where ^{137}A(x,y,z) is the ^{137}Cs activity at the location where the mass spectrometry sample was taken. LaGrange interpolation methods were used to determine ^{137}A(x,y,z) values.

The above analysis assumes that the ^{235}U burnup is proportional to the ^{137}Cs activity. Actually, it is proportional to the ^{137}Cs activity resulting from ^{235}U fissions. Thus, the measured activities were multiplied by a calculated ^{235}U fission fraction, ^{235}F/F. EPRI-CELL calculations were used to determine ^{235}F/F as a function of burnup. This correction tends to increase the fuel-clement- averaged burnup by about 1%.

An estimate of errors associated with this technique is given below.

Source	Error Estimate, %
Counting statistics and repeatability	1.2
Numerical Integration	1.6
Length of Fuel Column	1.5
Total (Quadrature):	2.5

It is assumed that errors in the determination of the uranium isotopic abundances are negligible. In regions of steep gradients (near fuel column ends) $^{137}A(x,y,z)$ values are subject to additional errors amounting to several percent.